



**HAL**  
open science

# First insights on the diversity of the genus *Ostreopsis* (Dinophyceae, Gonyaulacales) in Guadeloupe Island, with emphasis on the phylogenetic position of *O. heptagona*

Aurélie Boisnoir, G Bilien, Rodolphe Lemee, Nicolas Chomérat

► **To cite this version:**

Aurélie Boisnoir, G Bilien, Rodolphe Lemee, Nicolas Chomérat. First insights on the diversity of the genus *Ostreopsis* (Dinophyceae, Gonyaulacales) in Guadeloupe Island, with emphasis on the phylogenetic position of *O. heptagona*. *European Journal of Protistology*, 2022, 83, 10.1016/j.ejop.2022.125875 . hal-03945405

**HAL Id: hal-03945405**

**<https://hal.science/hal-03945405>**

Submitted on 22 Jul 2024

**HAL** is a multi-disciplinary open access archive for the deposit and dissemination of scientific research documents, whether they are published or not. The documents may come from teaching and research institutions in France or abroad, or from public or private research centers.

L'archive ouverte pluridisciplinaire **HAL**, est destinée au dépôt et à la diffusion de documents scientifiques de niveau recherche, publiés ou non, émanant des établissements d'enseignement et de recherche français ou étrangers, des laboratoires publics ou privés.



Distributed under a Creative Commons Attribution - NonCommercial 4.0 International License

1 **First insights on the diversity of the genus *Ostreopsis* (Dinophyceae,**  
2 **Gonyaulacales) in Guadeloupe Island, with emphasis on the phylogenetic**  
3 **position of *O. heptagona***

4 Aurélie BOISNOIR<sup>1</sup>, Gwenaél BILIEN<sup>2</sup>, Rodolphe LEMÉE<sup>3</sup> and Nicolas CHOMÉRAT<sup>2</sup>

5

6 <sup>1</sup>Ifremer, BIODIVENV, F-97231 Le Robert, Martinique, France

7 <sup>2</sup>Ifremer, LITTORAL, F-29900 Concarneau, France

8 <sup>3</sup>Sorbonne Université, CNRS, Laboratoire d'Océanographie de Villefranche, Villefranche-sur-Mer,

9 France

10

11 Corresponding authors:

12 N. Chomérat: [nicolas.chomerat@ifremer.fr](mailto:nicolas.chomerat@ifremer.fr)

13

14 ORCID

15 Gwenaél Bilien: 0000-0002-8633-3441

16 Rodolphe Lemée: 0000-0002-7800-2220

17 Nicolas Chomérat: 0000-0001-9691-6344

18

19 Abstract:

20 The present study aims to identify epiphytic *Ostreopsis* cells collected in Guadeloupe between 2017  
21 and 2018 using a morpho-molecular approach. This method combined microscopical observations  
22 of wild specimens (light and scanning electron microscopy) with a phylogenetic analysis inferred  
23 from concatenated sequences of ribosomal operon (SSU + ITS + LSU) of Ostreopsidoideae. Four  
24 distinct morphotypes were identified in our samples and studied by SEM. Molecular data obtained  
25 from single-cell PCR for the four morphotypes were consistent with observations and confirmed the  
26 presence of three *Ostreopsis* species resolved in well characterized genotypes (*O. cf. ovata*, *O.*  
27 *lenticularis* and *O. siamensis*) and an unidentified clade. Detailed morphological characters  
28 including sulcal plates confirmed the identification of the last morphotype as *O. heptagona*  
29 D.R.Norris, J.W.Bomber & Balech, which forms a new basal clade in the genus, not previously  
30 reported. Observations highlighted overlapping sizes for *O. lenticularis*, *O. siamensis* and *O.*  
31 *heptagona*. Direct sequencing of PCR products obtained for some *O. lenticularis* and *O. heptagona*  
32 collected at one site revealed unexpectedly the presence of the parasitoid dinoflagellate  
33 *Amoebophrya*. Some *Ostreopsis* cells were found partially emptied and exhibiting a compact mass.  
34 Further analyses are needed to understand the ecological role of *Amoebophrya* on blooms of  
35 epiphytic *Ostreopsis* species.

36

37 Keywords:

38 Concatenated phylogeny, morpho-molecular taxonomy, *Ostreopsis* cf. *ovata*, *Ostreopsis*  
39 *lenticularis*, *Ostreopsis siamensis*, ribosomal operon

40

41 Highlights:

42 Identification of four *Ostreopsis* species and characterization of a novel basal clade

43 Detailed SEM observations and rDNA sequencing of *Ostreopsis heptagona*

44 Detection of infected *Ostreopsis* spp. cells by the parasitoid *Amoebophrya*

## 45 **Introduction**

46 The dinoflagellate genus *Ostreopsis* Johs.Schmidt, 1901 had first been observed in plankton  
47 samples collected in the Gulf of Thailand (Schmidt, 1901) but has seldomly been reported since  
48 then, due to its predominantly benthic habitat (Besada et al., 1982). Owing to its co-occurrence with  
49 the genus *Gambierdiscus* in tropical regions (Fukuyo, 1981; Ballantine et al., 1985; Berland et al.,  
50 1992), this genus benefited from the interest on microalgae associated with the ciguatera poisoning  
51 (CP) which allowed the description of several species between the 1980's and the 1990's (Fukuyo,  
52 1981; Norris et al., 1985; Faust and Morton, 1995; Faust, 1999) and initiated the assessment of their  
53 toxicity (Ballantine et al., 1988; Tosteson et al., 1989; Berland et al., 1992). The toxins synthesized  
54 by *Ostreopsis* species are palytoxin-like molecules that can cause health issues especially in  
55 temperate areas (Gallitelli et al., 2005; e.g. Durando et al., 2007; Tichadou et al., 2010; Vila et al.,  
56 2016) where some species form recurrent blooms (Shears and Ross, 2009; Cohu et al., 2013;  
57 Ninčević Gladan et al., 2019; Açaçaf et al., 2020). Reports of *Ostreopsis* have become more and more  
58 frequent over the past decades (Shears and Ross, 2009; Shah et al., 2014; Park et al., 2020).  
59 Furthermore, palytoxin analogues can bio-accumulate in marine organisms (Biré et al., 2013, 2015)  
60 and constitute a significant risk for human health because of their potentially high toxicity and their  
61 thermostability (Katikou, 2007). Blooms are less frequently reported in tropical areas (Shears and  
62 Ross, 2009), but it has been shown that some species can reach high abundances and sometimes  
63 form benthic blooms (Chomérat et al., 2020b). Although palytoxin-like molecules have not been  
64 directly linked-with CP, they may be involved in poisoning derived from the ingestion of tropical  
65 marine organisms causing various symptoms reported in ciguateric endemic areas such as  
66 palytoxicosis and clupectoxism (Alcala et al., 1988; Onuma et al., 1999; Randall, 2005).

67 In terms of species diversity, the Caribbean basin appears as a particularly rich area where  
68 nine of the eleven currently described species included in the genus *Ostreopsis* (Guiry and Guiry,  
69 2021) have been reported from the Gulf of Mexico and the Caribbean Sea. Three species described  
70 from the Indo-Pacific area have been mentioned in the Caribbean, such as *O. siamensis*  
71 Johs.Schmidt (Bomber et al., 1988, 1989; Faust and Gullede, 1996), *O. ovata* Y.Fukuyo (Besada et  
72 al., 1982; Faust and Gullede, 1996; Faust, 2004) and *O. lenticularis* Y.Fukuyo (Ballantine et al.,  
73 1985, 1988; Tosteson et al., 1986, 1989; Faust, 1995, 2004; Faust et al., 1996; Delgado et al., 2006).  
74 Interestingly, five other species have been described from various areas of the Caribbean basin,  
75 including *O. heptagona* D.R.Norris, J.W.Bomber & Balech (Norris et al., 1985), *O. labens*  
76 M.A.Faust & S.L.Morton (Faust and Morton, 1995), *O. belizeana* M.A.Faust, *O. caribbeana*  
77 M.A.Faust and *O. marina* M.A.Faust (Faust, 1999). While the presence of *O. heptagona*, *O. labens*  
78 and *O. mascarenensis* Quod (Quod, 1994) has been suggested in various tropical areas (Faust and  
79 Morton, 1995; Faust et al., 1996), the other three species have never been unambiguously identified  
80 elsewhere than in their type localities. For instance the putative identification of *O. marina* in the

81 Indian Ocean (Carnicer et al., 2015) was unclear, and morphological and genetic data allowed to  
82 conclude that the species present in that region actually belongs to *O. lenticularis* (Chomérat et al.,  
83 2019b).

84 As stated previously, the morphological plasticity in *Ostreopsis* species led to some  
85 ambiguous identifications (Parsons et al., 2012; Hoppenrath et al., 2014; Chomérat et al., 2019b;  
86 Rhodes et al., 2020) and the existence of some *Ostreopsis* morphospecies has recently been  
87 questioned (Borsato et al., 2020; Chomérat et al., 2020b). In the Caribbean area, health risks  
88 associated with the toxicity of some *Ostreopsis* species have been reported (Norris et al., 1985;  
89 Tosteson et al., 1986; e.g. Ballantine et al., 1988), the identification of toxic species, however,  
90 remained unclear (Chomérat et al., 2019b), and further studies based on molecular data appear now  
91 necessary to resolve such issues (Sato et al., 2011; Tawong et al., 2014; Zhang et al., 2018). The use  
92 of molecular data from ribosomal DNA or internal transcribed spacers regions has proven to be  
93 extremely powerful to discriminate genotypes within the genus (e.g Penna et al., 2010; Sato et al.,  
94 2011; Tawong et al., 2014; Lee and Park, 2020). Still, association of genotypes with existing  
95 taxonomic descriptions was not always clear, since morphological data were lacking or not detailed  
96 enough for accurate characterization (Sato et al., 2011; Chomérat et al., 2020b). Only two species,  
97 *O. fattorussoi* Accoroni, Romagnoli & Totti and *O. rhodesiae* Verma, Hoppenrath & S.A.Murray  
98 include molecular data with their formal description (Accoroni et al., 2016; Verma et al., 2016), and  
99 recent re-investigations of *O. lenticularis*, *O. mascarenensis* and *O. siamensis* allowed to clarify  
100 their genetic identity (Chomérat et al., 2019b, 2020a; Nguyen-Ngoc et al., 2021). Combining  
101 morphological and genetic data from specimens acquired at or near the type localities appears as a  
102 major task to provide reliable taxonomic reference data for unambiguous identification of species  
103 (Parsons et al., 2012).

104 To date, there are no molecular studies on the genus *Ostreopsis* available from the Caribbean  
105 and there is a serious need of data to confirm the putatively high diversity inferred from  
106 morphological reports. Therefore, in the framework of a program aiming to explore the diversity of  
107 benthic dinoflagellates in the Caribbean Sea, the present study focuses on clarifying the taxonomic  
108 diversity of *Ostreopsis* in Guadeloupe Island based on a morpho-genetic approach. For the first  
109 time, single-cells of different morphotypes isolated from samples collected around the island were  
110 used for molecular sequencing of LSU rDNA. In addition, detailed morphological features were  
111 studied with high resolution scanning electron microscopy to assess species identifications. By  
112 combining morphological and molecular data, the present study allowed to better interpret the  
113 diversity around Guadeloupe Island, which constitutes a prerequisite for ecological studies of  
114 benthic communities associated with CP. Moreover, this study showed, in an unexpected manner,  
115 the infection of *Ostreopsis* cells by the parasitoid *Amoebophrya*.

## 116 **Material and Methods**

### 117 ***Sampling***

118 Samples were collected between July and October 2017 and in July 2018 at four sites in various  
119 parts of Guadeloupe Island: Bois Jolan, Chapelle, Le Gosier and Rivière Sens (Fig. 1). During the  
120 sampling, several macrophytes were carefully collected with surrounding water in 50 ml plastic  
121 tubes avoiding the resuspension of epiphytic microalgae growing on the thalli (Table 1). Acidic  
122 Lugol solution at 1% (v/v) was added to all samples to preserve the microalgae and 10 seconds  
123 agitation allowed benthic dinoflagellates to detach from the macrophyte (Jauzein et al., 2018).  
124 Then, the epiphytic suspension was passed through a 500 µm mesh to remove larger organisms and  
125 detritus. Samples were stocked in the dark at 4°C.

126

### 127 ***Light and scanning electron microscopy***

128 For scanning electron microscopy (SEM), cells were first individually isolated and concentrated in  
129 2 ml tubes containing water and a drop of formaldehyde to prevent the development of fungi. Then,  
130 cells were filtered on polycarbonate membrane filters (Millipore RTTP Isopore, 1.2 µm pore size,  
131 Millipore, Billerica, USA), rinsed in deionized water, and prepared according to Chomérat & Couté  
132 (2008). Dehydration was carried out in ethanol baths 15%, 30%, 50%, 70%, 95% vol. ethanol for  
133 about 20 min in each bath, and then several baths of absolute ethanol. Cells were then dried using  
134 an EMS 850 (Electron Microscopy Science, Hatfield, PA, USA) critical point drier. After gold-  
135 coating as in Chomérat et al. (2020b), SEM examinations were carried out using a Sigma 300 field-  
136 emission SEM (Carl Zeiss Microscopy GmbH, Jena, Germany) in full vacuum mode and with an  
137 electron acceleration of 2 kV. Cells were measured on SEM digital micrographs using ImageJ  
138 software (Rasband, 1997). Depth corresponds to dorso-ventral length (DV) and height to antero-  
139 posterior (AP) length. SEM images were presented on a uniform background using GNU Image  
140 Manipulation Program v.2.10.18. For dissection of thecal plates, isolated cells were placed in a  
141 small drop of water on a slide, covered with a coverslip, and a drop of sodium hypochlorite (5%  
142 final concentration) was deposited on the border. The coverslip was then gently pressed using a  
143 stick and dissociated thecal plates were observed at high magnification using a BX41 (Olympus,  
144 Tokyo, Japan) upright microscope equipped with DIC optics. The terminology used for thecal plates  
145 in this paper follows the hybrid system of Hoppenrath et al. (2014) and Norris et al. (1985) for some  
146 sulcal plates.

147

### 148 ***Single-cells isolation, DNA amplifications and sequencing***

149 For molecular characterization, single-cells were isolated from preserved field-samples as described  
150 in Chomérat et al. (2019a). In order to focus on the diversity of *Ostreopsis* species in each site,

151 samples were analysed by sampling site, indistinctively of the macrophyte substratum. To resuspend  
152 epiphytic cells, the tube containing Lugol-fixed material was vigorously shaken and a subsample of  
153 30 µl was diluted in 4 ml of filtered seawater in a small Petri dish. Each cell of interest was isolated  
154 with a micropipette under an inverted microscope (Olympus IX51, Tokyo, Japan) measured and  
155 photographed with a camera (Olympus E-300 digital, Tokyo, Japan). Then, the cells were rinsed in  
156 four drops of distilled water before being transferred into a 200 µl PCR tube containing 5 µl of PCR  
157 grade distilled water. This process allowed to associate the morphology of a specimen with its  
158 sequence (Chomérat et al., 2019a). Tubes containing single-cells were stored at -20 °C until further  
159 analysis. A nested Polymerase chain reaction (PCR) was used for the amplification of one or two  
160 regions of the large subunit of ribosomal DNA (rDNA) (D1–D3 and D8–D10 domains). The first  
161 round of PCR used ITS-FW and RB primers (Table S1) then a second round of PCR was carried out  
162 using 1 µl of the amplicon produced in the first round, allowing the separate amplification of the  
163 D1–D3 and D8–D10 regions. PCR reactions were carried out in 20 µl using KOD Hot Start Master  
164 Mix (Novagen-Merck KgaA, Darmstadt, Germany), according to the manufacturer's instructions.  
165 The PCR cycling comprised an initial 2 min heating step at 95 °C to activate the polymerase,  
166 followed by 35 cycles of 95 °C for 20 s, 56 °C for 20 s, and 70 °C for 2 min. Primers used were  
167 D1R and D3B for D1–D3 domain and D8 and OstD10R for D8–D10 domain (Table S1). To obtain  
168 sequences of the parasitoid, a specific primer (AmoebR) has been designed from preliminary  
169 sequence results obtained with universal primers, and used to amplify specifically SSU–ITS region  
170 of the parasitoid (Table S1). PCR products were visualized on a 1% agarose gel after  
171 electrophoresis and the positive samples were purified using the ExoSAP-IT PCR Product Cleanup  
172 reagent (Affymetrix, Cleveland, OH, USA).

173 To confirm parasitoid and host sequences from infected specimens, a cloning step has been  
174 added. To allow a better ligation of the amplicon, the second PCR round was carried out using Taq  
175 polymerase (Promega PCR master mix) and primers ITS-FW–D3B with an initial 2 min heating  
176 step at 95 °C to activate the polymerase, followed by 20 cycles of 95 °C for 20 s, 60 °C for 20 s,  
177 and a final extension at 70 °C for 2 min. After confirmation by agarose gel electrophoresis, positive  
178 PCR products were purified using NucleoMag kit (Macherey-Nagel) and cloning was performed  
179 using pGEM<sup>®</sup>-T Easy Vector Systems kit and JM109 Competent Cells (Promega) according to the  
180 manufacturer's instructions. Positive clones were extracted with PureLink Quick Plasmid Miniprep  
181 kit (Invitrogen).

182 The Big Dye Terminator v3.1 Cycle Sequencing Kit (Applied Biosystems, Tokyo, Japan)  
183 was used for sequencing purified PCR products. Primers and excess dye-labeled nucleotides were  
184 first removed using the Big Dye X-terminator purification kit (Applied Biosystems, Foster City,  
185 CA, USA). Sequencing products were run on an ABI PRISM 3130 Genetic Analyzer (Applied  
186 Biosystems). Forward and reverse reads were obtained.

187

188 ***Sequences alignment and phylogenetic analyses***

189 *Ostreopsis* sequences of the LSU D1-D3, D8-10 and additionally ITS region for morphotype 4  
190 acquired in the present study were used in a multi-loci phylogenetic analysis following the most  
191 recent taxonomic treatment of gonyaulaceans by Tillmann et al. (2021), and including sequences of  
192 the three genera encompassed in subfamily Ostreopsidoideae Gottschling, Tillmann and Elbrächter.  
193 For that purpose, 138 sequences of *Ostreopsis* spp., *Coolia* spp. and *Alexandrium* spp. from the  
194 analysis by Tillmann et al. (2021) served as a basis to construct our matrix, using *Triadinium*  
195 *polyedricum* (2 sequences) and *Pyrodinium bahamense* (3 sequences) as outgroup. Sequences  
196 acquired on 25 different specimens in the present study and 21 *Ostreopsis* spp. sequences retrieved  
197 from GenBank were added to complete the genus diversity. Full voucher information of the  
198 systematically representative set comprising 184 gonyaulacean Ostreopsidoideae (84 *Ostreopsis*  
199 spp., 30 *Coolia* spp., 70 *Alexandrium* spp.) and outgroup (2 Gambierdiscoideae Fensome,  
200 F.J.R.Taylor, G.Norris, Sarjeant, Wharton & G.L.William, 3 Pyrodinioideae F.J.R.Taylor, G.Norris,  
201 Sarjeant, Wharton & G.L.William) are provided in Table S2. As described in Tillmann et al. (2021),  
202 for alignment constitution, separate matrices of the rRNA operon (i.e. SSU, ITS region and LSU)  
203 were constructed, aligned using MAFFT v. 7 (Kato and Standley, 2013) and concatenated  
204 afterwards using Seaview v. 5.05 software (Gouy et al., 2010). After concatenation, the matrix was  
205 refined by eye with Linux version of MEGA software v. 10.1.7 (Kumar et al., 2018).

206 A second dataset was prepared to analyse the phylogenetic position of the parasitoid  
207 *Amoebophrya* sp. infecting some *Ostreopsis* specimens. A matrix including small subunit of  
208 ribosomal RNA (SSU) and internal transcribed spacer 1 was prepared, using closely related  
209 sequences retrieved in GenBank, some sequences covering only SSU. They were aligned with  
210 MUSCLE algorithm (Edgar, 2004) followed by refinement by eye.

211 Prior to phylogenetic analyses, jModeltest2 v. 2.1.7 (Darriba et al., 2012) was used to search  
212 for the most appropriate model of sequence evolution. Two methods of phylogenetic reconstruction  
213 were used. Maximum Likelihood analysis (ML) was performed using PHY-ML v. 3 software  
214 (Guindon et al., 2010), and a bootstrap analysis (500 pseudoreplicates) were to assess the relative  
215 robustness of branches of the ML tree. Bayesian Inference analysis (BI) was carried out using  
216 MrBayes 3.1.2 software (Ronquist and Huelsenbeck, 2003). Parameters used to run phylogenetic  
217 calculations are given in supplementary Table S3. Nomenclature of clades (genotypes) follows that  
218 proposed by Sato et al. (2011) and subsequently by Tawong et al. (2014) and Chomérat et al.  
219 (2019b, 2020b).

220

221

## 222 Results

### 223 *Morphological observations*

224 Based on their size and appearance, assignment to four distinct morphotypes was possible. Cells of  
225 the morphotype 1 were small and conspicuously tear-shaped (Figs 2, 3A–B, 7A). The morphotype 2  
226 included broadly large oval cells with a regular margin (Figs 2, 3–I, 7B–E) while the morphotype 3  
227 corresponded to cells with a similar size and shape as morphotype 2 but with an irregular undulated  
228 margin and a twisted aspect (Figs 2, 4A–B, 7F–J). Finally, cells of morphotype 4 were large and  
229 tear-shaped (Figs 2, 5A–B, 6A, 7K–O). Morphotype 2 was found at CH, BJ and RS sites,  
230 morphotype 3 was only found at GO and RS sites, while morphotypes 1 and 4 were only present at  
231 RS and CH sites, respectively. Owing to these morphological peculiarities and their observation at  
232 certain stations, cells of the four morphotypes could be retrieved in the samples analysed by SEM,  
233 allowing further detailed observations of their characters. All cells were found to possess the typical  
234 plate pattern of the genus *Ostreopsis*, APC 3' 7'' 6?c ?s 5''' 2'''''. In the following descriptions, only  
235 significant distinctive morphological features are emphasized for each morphotype.

236

#### 237 Morphotype 1 - *Ostreopsis* cf. *ovata* Y. Fukuyo

238 Cells were ovate (Figs 3A–B, 7A), 43.2–52.3  $\mu\text{m}$  (mean  $\pm$  SD:  $48.1 \pm 3.5 \mu\text{m}$ ,  $n = 10$ ) deep (dorso-  
239 ventral length), 24.1–34.4  $\mu\text{m}$  wide (mean  $28.2 \pm 3.0 \mu\text{m}$ ,  $n = 10$ ). The length to width ratio varied  
240 from 1.52 to 1.87 (mean 1.71,  $n = 10$ ) (Figs 3A– B). The apical pore complex (APC) was composed  
241 of a slightly curved Po plate of about 8  $\mu\text{m}$  that was supported by a long 2' plate reaching the 4''  
242 plate dorsally (Fig. 3C). The cingulum was almost straight and deep (Figs 3D–E). The thecal  
243 surface was smooth and covered by thecal pores of 0.25–0.32  $\mu\text{m}$  in diameter without collar rim  
244 (Figs 3F–G). Interestingly, some rare smaller thecal pores (*ca.* 50 nm in diameter) were visible on  
245 the surface of plates (Figs 3F–G).

246

#### 247 Morphotype 2 - *Ostreopsis lenticularis* Y. Fukuyo

248 Cells were large, lenticulate in shape and broadly ovate (Figs 3H–I, 7B). Cells were 65.0–119.9  $\mu\text{m}$   
249 deep (mean  $\pm$  SD:  $95.8 \pm 12.8 \mu\text{m}$ ,  $n = 25$ ) and 56.2–96.9  $\mu\text{m}$  wide (mean  $\pm$  SD:  $77.8 \pm 11.2 \mu\text{m}$ ,  $n$   
250  $= 25$ ). The length to width ratio varied from 1.11 to 1.39 (mean  $\pm$  SD:  $1.23 \pm 0.08$ ,  $n = 25$ ). The  
251 APC was composed of a slightly curved Po plate of 15.8–18.2  $\mu\text{m}$  (mean  $\pm$  SD:  $17.0 \pm 1.2 \mu\text{m}$ ,  $n =$   
252 5) (Fig. 3J). The first apical plate 1' was rather large and six-sided (Fig. 5H). The second apical  
253 plate 2' was short and did not reach the 4'' plate (Fig. 3J) . The cingulum was straight in lateral view  
254 (Figs 3K–L). The thecal surface was covered with two kinds of pores without collar rim (Fig. 3M).  
255 The large pores were 0.3–0.4  $\mu\text{m}$  in diameter and the small pores were 90–150 nm in diameter.  
256 They were both present densely on the thecal surface.

258 Morphotype 3 - *Ostreopsis siamensis* Johs. Schmidt

259 Cells were broadly ovoidal (Figs 4A–B, 7F). They were 58.6–97.6  $\mu\text{m}$  deep (mean  $\pm$  SD: 80.4  $\pm$   
 260 11.1  $\mu\text{m}$ , n = 16) and 43.3–82.5  $\mu\text{m}$  wide (mean  $\pm$  SD: 66.1  $\pm$  11.7  $\mu\text{m}$ , n = 16). The length to width  
 261 ratio varied from 1.04 to 1.50 (mean: 1.23, n = 16). The APC was composed of a slightly curved Po  
 262 plate whose length varied from 14.8 to 17.9  $\mu\text{m}$  (mean  $\pm$  SD: 16.8  $\pm$  1.0  $\mu\text{m}$ , n = 8) (Fig. 4C). The  
 263 first apical plate was six-sided (Fig. 4A).. The second apical plate 2' was narrow, extending to  
 264 contact the 4'' plate (Fig. 4C). Ventrally, the cingulum appeared oblique and formed a V-shape (Fig.  
 265 4D). Cells appeared bulging in the median part of the epitheca (height: 30.6–41.7  $\mu\text{m}$ , n = 5) and  
 266 thinner near the edges (Figs 4E–F, G). In lateral view, the cingulum was conspicuously undulated,  
 267 giving a somewhat twisted aspect to the cells (Figs 4E–F). In the sulcal area, cells exhibited the  
 268 ventral opening (Vo), the anterior left sulcal plate (Ssa), the anterior right sulcal plate (Sda) and the  
 269 posterior sulcal plate (Sp) (Fig. 4H). On the hypotheca, plate 2'''' had typical curved shape (Figs 6B,  
 270 F) due to the cell twist. The thecal surface was covered with large pores (*ca.* 0.3  $\mu\text{m}$  in diameter)  
 271 surrounded by a shallow elevated rim and some very small pores (*ca.* 50–60 nm in diameter) were  
 272 also present at a lower density (Fig. 4I).

273

274 Morphotype 4 - *Ostreopsis heptagona* D.R.Norris, J.W.Bomber & Balech

275 Cells were large, and typically tear-shaped (Figs 5A–B, 6A, 7K– O, S1). They were 77.9–110.5  $\mu\text{m}$   
 276 deep (mean  $\pm$  SD: 95.1  $\pm$  6.2  $\mu\text{m}$ , n = 45) and 45.7–75.2  $\mu\text{m}$  wide (mean  $\pm$  SD: 60.0  $\pm$  6.8  $\mu\text{m}$ , n =  
 277 43). The length to width ratio varied from 1.39 to 1.80 (mean  $\pm$  SD: 1.56; n = 43). The APC was  
 278 composed with a slightly curved Po plate 14.6–17.2  $\mu\text{m}$  long (mean  $\pm$  SD: 16.1  $\pm$  0.9  $\mu\text{m}$ ; n = 8)  
 279 with the apical pore consisting in a slit encircled by a row of thecal pores partially visible (Figs 5D,  
 280 6B). The epithelial surface examination of this morphotype revealed a conspicuous seven-sided (i.e.  
 281 heptagonal) 1' plate making contacts with plates Po, 3', 1'', 2'', 5'', 6'' and 7'' (Figs 5A, C). The  
 282 second apical plate 2' was narrow and elongated and reached the 4'' plate dorsally (Fig. 5D). Plate 3'  
 283 was pentagonal (Fig. 5A). Precingular plates were unequal in size, with plates of the right side (i.e.  
 284 4'', 5'', 6'' and 7'') higher than those of the left side (Figs 5A,F). On the left side, plate 3'' was the  
 285 smaller of the series. Among precingular plates, 1'', 3'', 6'' and 7'' were four-sided, in contrast with  
 286 2'', 4'' and 5'' which were pentagonal.

287 The cingulum appeared almost closed and straight in all studied specimens, and no cingular  
 288 plates could be distinguished in SEM (Figs 5E–F, S1). In LM, some cingular plates (c1; c2)  
 289 appeared very narrow (Figs 6B, D, E). The sulcus was small and narrow (Figs 5F–G). Ventrally, the  
 290 ventral opening (Vo) was visible in contact with 1'' plate (Figs 5F–G, 6A, D). From SEM  
 291 observations, only three sulcal plates could be resolved and some were obscured by the overlap of  
 292 1'''' plate (Fig. 5G). Observation of dissected cells at high magnification in LM allowed to complete

293 the sulcus description and four additional plates could be observed (Figs 6C–I). The most  
294 conspicuous plates both in LM and SEM were the anterior left sulcal plate (Ssa) which appeared  
295 elongated and in contact with Vo and 1'' on the epitheca, while it extended on the left within the  
296 cingular furrow (Figs 5G, 6D, H) and the anterior right sulcal (Sda), elongated located below Ssa  
297 and forming a prominent list (Figs 5G, 6D, H). These two plates had a complex three dimensional  
298 structure, and appeared conspicuously curved when seen from top (Figs 6D–E, H–I). On the left  
299 side of Ssa, a deeply recessed plate with a squared shape on the right and a rounded indentation  
300 with a thick edge on the left margin, was present and interpreted as a 't' plate (Fig. 6G). Just below  
301 this plate, a rectangular posterior left sulcal (Ssp) plate was observed in contact with Ssa, Sda (Fig.  
302 6H). A small elongated and almost triangular (Fig. 6E) posterior right sulcal plate (Sdp) was in  
303 inserted between Ssp and the posterior sulcal plate (Sp) which was six-sided, and with a hyaline  
304 part where it was overlapped by 1'''' (Fig. 6F). Finally, the dissection revealed that a ring-shaped  
305 plate delimiting Vo could detach from the Ssa (Fig. 6I), and it could be interpreted as an anterior  
306 sulcal plate (Sa).

307 The hypotheca comprised seven major plates unequal in size (Fig. 5B). Seen antapically, the  
308 2''''/3'''' and 4''''/5'''' sutures appeared roughly at the same level (Fig. 5B). Plate 1'''' was in contact  
309 with 1''', 2''', 2'''' and overlapped the sulcal area (Fig. 5B, G, S1). Plate 2'''' was pentagonal with  
310 contacts with 1''', 3''', 1''''', 2'''''' plates and the cingulum. Furthermore, this plate was broader on its  
311 dorsal part, giving an asymmetrical shape (Fig. 5B, S1). Plates 3'''' and 4'''' were both four-sided and  
312 roughly of the same size (Fig. 5B, S1). Four-sided plate 5'''' had the most distinctive shape with its  
313 long and curved suture in contact with plate 2'''''' and its narrower size ventrally (Figs 5B, S1).

314 Interestingly, in the population from sample CH1, we noticed some variations of the  
315 hypothecal pattern of some specimens, while no variation was seen on epithecae. On these  
316 particular cells, a small extra plate was found on the ventral part of 2'''''' plate, in contact with 1''''  
317 and Sp plates (Fig. S1). Plate 2'''''' of these specimens appeared to be split obliquely on its ventral  
318 left side, with the larger part (2'''''' $\alpha$ ) dorsal and six sided, and the smaller part (2'''''' $\beta$ ) ventral and  
319 four-sided and more or less reduced (Fig. S1).

320 The thecal surface was homogeneously covered with a single type of pores *ca.* 0.3–0.4  $\mu$ m  
321 in diameter (Fig. 5H). Some larger pores up to 0.5  $\mu$ m were occasionally observed on some  
322 specimens (e.g. on plates 2'''' and 3''''', Fig. 5B).

323

### 324 *Single-cells isolation and phylogenetic analysis*

325 For the phylogenetic analysis of Ostreopsidoideae, the alignment comprised 189 OTUs including 25  
326 specimens from Guadeloupe Island (Figs 7A– O) and was 6382 bp (1896 + 815 + 3671) long  
327 including gaps. It comprised 631 + 637 + 1352 parsimony-informative sites and 3785 distinct  
328 PhyML alignment patterns.

329 The ML majority-rule consensus tree is shown on Fig. 8 and topologies were largely  
330 congruent regardless of whether ML or bayesian inference methods were used. The genus  
331 *Ostreopsis* was monophyletic and fully supported among other Ostreopsidoideae (Figs 8, S2).  
332 *Coolia* formed a sister clade to *Ostreopsis* while *Alexandrium* appeared more basal (Figs 8, S2).  
333 Among *Ostreopsis*, 13 major lineages that corresponded to established taxa at species rank were  
334 resolved and well to fully supported (Fig. 8): *O. cf. ovata*, *O. rhodesiae*, *O. mascarenensis*, *O.*  
335 *fattorussoi*, *O. lenticularis*, *O. siamensis*, *O. heptagona* and *Ostreopsis* sp. 1/2-4, 7-10 (Fig. 8).  
336 Sequences acquired from the four different morphotypes in the present study (Figs 7A–O) were  
337 resolved within four major clades (Fig. 8). One sequence was recovered in *O. cf. ovata* clade, 11 in  
338 *O. lenticularis* clade, 6 in *O. siamensis* clade, and 7 in *O. heptagona* clade. Sequences of *O. cf.*  
339 *ovata*, *O. lenticularis* and *O. siamensis* from Guadeloupe Island were closely related to sequences  
340 already available in GenBank and thus represent known genotypes (Fig. 8). Within *O. lenticularis*  
341 clade, all sequences from Guadeloupe Island were closely related to those from French Polynesia  
342 (type locality) (Fig. 8). Among sequences of *O. siamensis*, the 6 sequences from the present study  
343 were resolved with a strong support with sequences from the Gulf of Thailand (TF25OS,  
344 VNPQ218) and Tahiti Island (PNA19-6, PNA19-8 and IFR20-173). By contrast, sequences of *O.*  
345 *heptagona* were all similar and clustered in a new clade, sister of all other *Ostreopsis* lineages,  
346 which did not include any sequence from GenBank (Fig. 8). This clade was basal to all other  
347 *Ostreopsis* sequences but it was fully recovered within *Ostreopsis* genus based on the concatenated  
348 analysis (100BS, 1.00PP). Phylogenetic analyses inferred from single locus sequences (ITS and  
349 LSU D1-D3 + D8-D10) are given in supplementary figures S3 and S4. While the exact same  
350 position was found for this clade, the support was less robust than in the concatenated analysis  
351 presented herein.

### 352 353 ***Detection of infected Ostreopsis spp. cells by the parasitoid Amoebophrya sp.***

354 Direct sequencing of PCR products obtained for some specimens from sample CH1 (Table 1)  
355 unexpectedly revealed the presence the parasitoid dinoflagellate genus *Amoebophrya* which has not  
356 been previously recognized when isolating single-cells. This preliminary result indicated a possible  
357 contamination or the presence of this parasitoid in the sample, but contamination was excluded as  
358 several independent PCR analyses revealed the same finding. Since partial LSU sequences obtained  
359 were not useful enough for identification and phylogenetic analysis of the parasitoid, a more  
360 thorough investigation has been undertaken to confirm this result. New specimens have been sought  
361 in the Lugol-fixed sample CH1 for amplification of SSU–ITS region. Observed carefully with light  
362 microscope, some *Ostreopsis* cells were found to have a peculiar appearance and seemed partially  
363 emptied with gaps in their cytoplasm, and they exhibited a compact mass, more or less developed  
364 and located dorsally (Figs 9A–F). This typical feature has been observed both in *O. lenticularis*

365 (Figs 9A–D) and *Ostreopsis heptagona* (Figs 9E–F). For putatively infected specimens of *O.*  
366 *lenticularis* (IFR18-618, IFR18-622, IFR18-624), only sequences of the parasitoid were obtained.  
367 In case of the specimen IFR17-685 of *Ostreopsis heptagona* (Fig. 7N), sequences of both the  
368 parasitoid and the host were obtained. The four sequences of *Amoebophrya* sp. infecting *Ostreopsis*  
369 spp. (accession numbers MW363873–MW363876) were identical. In the ML-tree (Fig. 10), they  
370 were resolved with strong support with the sequence MK752531.1 of an isolate (AT5) for which the  
371 host was not identified. From the phylogenetic analysis, it appeared that among the great genetic  
372 diversity within *Amoebophrya*, the parasitoid identified in this study belongs to a clade distantly  
373 related to other genotypes known to infect other planktonic dinoflagellates genera such as  
374 *Akashiwo*, *Alexandrium*, *Ceratium* (=Tripos), *Cochlodinium*, *Dinophysis*, *Gonyaulax*,  
375 *Gymnodinium*, *Karlodinium*, *Phalacroma*, *Prorocentrum* and *Scrippsiella* (Fig. 10).

376

## 377 Discussion

### 378 Phylogeny and species identities

379 Results from morphotype observations and phylogenetic analysis confirm the presence of four  
380 *Ostreopsis* species in the samples studied from Guadeloupe Island. The concatenated tree reveal a  
381 similar topology than found in the recent study by Tillmann et al. (2021), and *Ostreopsis* is a well  
382 resolved genus among subfamily Ostreopsidoideae. Within *Ostreopsis* clade, the topology is also  
383 congruent with previous studies based on single locus data (e.g. Chomérat et al., 2019b, 2020b;  
384 Sato et al., 2011; Tawong et al., 2014) and using a longer dataset provides a stronger support for  
385 several clades. While three of the genotypes from Guadeloupe Island cluster unambiguously within  
386 already known clades of *Ostreopsis* (*O.* cf. *ovata*; *O.* *lenticularis* and *O.* *siamensis*), the analysis  
387 reveals a novel basal clade not previously identified in any other study and for which the identity  
388 needs to be clarified.

389 As confirmed by molecular data, smaller cells of morphotype 1 correspond to *O.* cf. *ovata*,  
390 and compared with existing morphological data for *O.* cf. *ovata*, cells from Guadeloupe Island are  
391 in the size range reported for this species from various areas (e.g. Fukuyo, 1981; Penna et al., 2010;  
392 Zhang et al., 2018; Junqueira de Azevedo Tibiriçá et al., 2019; Nascimento et al., 2020). The  
393 detailed morphological analysis by SEM also confirms the plate pattern and characters observed  
394 previously (Fukuyo, 1981; Junqueira de Azevedo Tibiriçá et al., 2019). Nevertheless, observations  
395 at high magnification show the presence of very small thecal pores (ca. 50 nm) on the surface of  
396 thecal plates, as recently reported by Tibiriçá et al. (2019). Hence, this confirms that this species  
397 possesses a few small pores, as in other species such as *O.* *lenticularis* (Fukuyo, 1981; Chomérat et  
398 al., 2019b), *O.* *rhodesiae* (Verma et al., 2016) or in *O.* *siamensis* (Chomérat et al., 2020b; Nguyen-  
399 Ngoc et al., 2021). These small pores are however rare and quite difficult to observe, and they may

400 be present in certain strains only, which may explain the variability reported in different studies  
401 (e.g. Hoppenrath et al., 2014). Genetically, the unique sequence from Guadeloupe is not identical  
402 with any strain from GenBank and it might constitute a different ribotype.

403 Cells of morphotype 2 identified as *O. lenticularis* have the typical morphology of this large  
404 species, with wide and sometimes almost round cells. The size variation observed in specimens  
405 from Guadeloupe is larger than reported in any other study, exceeding the ranges 60–100  $\mu\text{m}$  in  
406 depth and 45–80  $\mu\text{m}$  in width given by Fukuyo (1981) in the original description. Interestingly,  
407 Faust et al. (1996) reported larger sizes for *O. lenticularis*, although it was obviously misidentified  
408 as '*O. siamensis*', as emphasized by Chomérat et al. (2019b). Using specimens from various  
409 populations worldwide including the Caribbean Sea, the Indian Ocean and the Japanese Pacific  
410 Ocean, these authors reported 108–123  $\mu\text{m}$  in depth and 76–86  $\mu\text{m}$  in width, but in absence of  
411 location data it is impossible to know if there was a pattern linked with geographical origin. From  
412 these values, the size variation appears quite low, in contrast with the observations by Zhang et al.  
413 (2018) who reported specimens 68.0–113.5  $\mu\text{m}$  deep and 56.5–97.3  $\mu\text{m}$  wide in their study from  
414 Hainan Island, or in the present study. Faust et al. (1996) apparently did not find cells smaller than  
415 108  $\mu\text{m}$  deep which is already a very large size for this species, compared with its original  
416 description (Fukuyo, 1981; Chomérat et al., 2019b). However, it is noteworthy that such large  
417 specimens as observed by Faust et al. (1996) are present in Guadeloupe Island, and the present  
418 study reveals that they are genetically identical to other sequences of *O. lenticularis*, which suggests  
419 that all belong to the same species. As mentioned by Fukuyo (1981) and later by Chomérat et al.  
420 (2019b), the major thecal characters of this species are a straight cingulum, and the typical presence  
421 of large and small pores, the latter being very abundant. All these features are present in the  
422 specimens from Guadeloupe Island and no difference has been found with other data.

423 The last species clearly identified by morphology (morphotype 3) and molecular data is *O.*  
424 *siamensis*, which has been recently reinvestigated by Nguyen-Ngoc et al. (2021). Prior to this study,  
425 this genotype was referred as to *Ostreopsis* sp. 6 (Sato et al., 2011; Tawong et al., 2014; e.g.  
426 Chomérat et al., 2020b; Lee and Park, 2020). Cells are large, undulated with a sigmoid cingulum  
427 and large thecal pores are surrounded by a shallow elevated rim (Chomérat et al., 2020b; Nguyen-  
428 Ngoc et al., 2021). All these features correspond well to the observations in Guadeloupe Island, but  
429 the cell undulation was even more pronounced, giving an asymmetrical shape of the cells, visible  
430 even with light microscope. Regarding size, cells from Guadeloupe Island are almost in the same  
431 range than in Tahiti Island (cells 58.0–82.5  $\mu\text{m}$  deep and 45.7–61.2  $\mu\text{m}$  wide), but larger specimens  
432 have been found in the present study. Compared with data for *O. siamensis* (excluding *O. cf.*  
433 *siamensis* which is another species, Chomérat et al. 2020b; Nguyen-Ngoc et al. 2021), cell sizes  
434 from Guadeloupe are remarkably similar to measurements given by Fukuyo (1981) from Japanese  
435 populations. Compared with data by Faust et al. (1996), considering the misidentification between

436 *O. lenticularis* and *O. siamensis* by these authors (Chomérat et al., 2020b), a wider size range is  
437 observed in Guadeloupe Island. However, if data of *O. labens* and *O. siamensis* in Faust & Morton  
438 (1995) and Faust et al. (1996), are merged to consider a single species, the resulting size range  
439 becomes remarkably similar with our data, with cells 65–98  $\mu\text{m}$  deep and 57–80  $\mu\text{m}$  wide. As  
440 already pointed out by Chomérat et al. (2020b), larger sizes reported by Faust & Morton (1995) for  
441 *O. labens* must be regarded cautiously as the sizes measured on some micrographs using scale bars  
442 are outside the range given in the text. In addition, Chomérat et al. (2020b) questioned the existence  
443 of *O. labens* because morphology was not significantly different from *O. siamensis*, but it may be  
444 cryptic and belongs to one of the subclades within *O. siamensis* (Chomérat et al., 2020b).  
445 Additional sequences from the Caribbean region are necessary to resolve this question and present  
446 data from Guadeloupe Island, eastern Caribbean, bring new elements to help clarifying this issue.  
447 The fact that all sequences obtained in this study are almost identical and cluster with strong support  
448 with sequences from the Gulf of Thailand (TF39OS, VNPQ218) and Tahiti Island indicate  
449 unambiguously that all belong to *O. siamensis* since strain VNPQ218 from Phu Quoc has been  
450 recently proposed as epitype by Nguyen-Ngoc et al. (2021). Nevertheless, a different genotype  
451 putatively corresponding to *O. labens* may be present in Belize and absent in Guadeloupe Island,  
452 and molecular data from Belize (type locality of *O. labens*) are absolutely necessary to clarify its  
453 existence or its junior synonymy with *O. siamensis*.

454

#### 455 ***Identification of the morphotype 4 as O. heptagona***

456 The morphology of morphotype 4 in Guadeloupe Island fits almost perfectly with the description of  
457 *O. heptagona* from Knight Key, Florida (Norris et al., 1985). Regarding size, Norris et al. (1985)  
458 described it as a large species, 96–122  $\mu\text{m}$  (average 108  $\mu\text{m}$ ) deep and 62–84  $\mu\text{m}$  (average 70  $\mu\text{m}$ )  
459 wide. Cell sizes in the present study are in the same range, although no specimen reached the higher  
460 values reported by Norris et al. (1985), while smaller cells have been observed in Guadeloupe  
461 Island. By comparison, Faust et al. (1996) reported smaller cells of *O. heptagona* in Belize, where  
462 size was 80–108  $\mu\text{m}$  deep and 46–59  $\mu\text{m}$  wide, and their lower values are in agreement with  
463 smaller specimens in our observations. Overall morphology and plate pattern of cells from  
464 Guadeloupe Island are similar to the description by Norris et al. (1985). The most striking character  
465 of this species is the presence of a conspicuous suture between 1' and 5'' plates, giving a heptagonal  
466 shape to 1' plate. Although this pattern has sometimes also been observed in teratological specimens  
467 of cultured *O. cf. ovata* (Besada et al., 1982; Penna et al., 2010), our observations reveal that it is an  
468 unambiguous character in all observed specimens. The shape and the number of sulcal plates  
469 observed match with the description of *O. heptagona* made by Norris et al. (1985) which confirm  
470 the identification of this species. Another conspicuous feature is the very narrow cingulum, almost

471 closed, which is also a character mentioned by Norris et al. (1985) who reported a width of *ca.*  
472 1.5–3.0  $\mu\text{m}$ .

473 In contrast with *O. lenticularis* or *O. siamensis* recently observed in detail with SEM (Chomérat et  
474 al., 2019b, 2020b), the small posterior right sulcal plate (Sdp) which inserts between Sda and Sp  
475 plates has not been observed in any specimen from Guadeloupe Island, and if present, it is  
476 completely hidden by the overlap of 1<sup>'''</sup> plate. Previous SEM observations of this species are  
477 scarce. Faust et al. (1996) provided illustrations showing only partially the morphology of *O.*  
478 *heptagona*, and they observed one type of thecal pores (0.3  $\mu\text{m}$  in diameter) which is similar with  
479 our data. Surprisingly, Accoroni et al. (2020) recently mentioned the use of SEM for identification  
480 of this species in Florida, but they did not provide any image nor molecular data preventing from  
481 any comparison. From all aforementioned, morphological characters of cells from Guadeloupe  
482 Island are in good agreement with the description of *O. heptagona*, and to our knowledge, the  
483 present study is the first to combine detailed SEM observations and DNA sequences of this species.  
484 However, since our material from Guadeloupe Island was relatively distant from type locality (*ca.*  
485 2,250 km southeast from Knight Key), it would be important to obtain sequences from this area.

486         Interestingly, our observations of many cells from the population of Chapelle sample reveal  
487 some specimens with an aberrant hypothecal pattern, in particular with a split 2<sup>'''</sup> plate, which has  
488 not previously been reported from field specimens of *O. heptagona*. Variations in the thecal plate  
489 pattern of dinoflagellates and existence of split plates is not unusual and this has been mentioned in  
490 several genera (e.g. Besada et al., 1982; Chesnick and Cox, 1985; Chomérat and Couté, 2008). Such  
491 variations concern more generally the epitheca than the hypotheca that is generally considered as  
492 more stable (Chesnick and Cox, 1985), so the present result seems contradictory. Since the sample  
493 in which specimens with additional plates have been found is also containing numerous infected  
494 cells by the parasitoid *Amoebophrya* (Syndiniales), it can be hypothesized that thecal variations  
495 occur more frequently in parasited host cells, but further investigations would be necessary confirm  
496 this fact.

497

#### 498 ***Diversity and comparison with data from the Caribbean***

499 As discussed previously by Chomérat et al. (2019b), several confusions have been made regarding  
500 *O. siamensis* and *O. lenticularis* in different studies, and in most reports the correct identification  
501 was not ascertained. For instance, the name change from *O. siamensis* in Carlson (1984) to *O.*  
502 *lenticularis* in Carlson & Tindall (1985) in the interpretation of the same dataset introduced some  
503 confusions which have been encouraged by the speculative statement by Norris et al. (1985) who  
504 considered the two species as possibly conspecific without any detailed argument. Some subsequent  
505 reports from the Caribbean area (e.g. Ballantine et al., 1985; Tosteson et al., 1986, 1989) do not  
506 provide a clear identification of *Ostreopsis* species and the identity of the studied species remains in

507 question. It cannot be excluded that several co-existing species have been misidentified and referred  
508 as to a single name. In 1990, Tindall et al. (1990) examined toxic clonal strains from U.S. Virgin  
509 Islands ascribed to '*O. lenticularis*' with SEM and realized that morphologically cells better  
510 correspond with the description of *O. siamensis*, but considering that this species had not been  
511 mentioned from the Caribbean, they intentionally continued with the misidentification of *O.*  
512 *lenticularis*, making the identity of the toxic species doubtful. Interestingly, using LM only,  
513 Gamboa Márquez et al. (1994) were able to accurately identify both *O. siamensis* and *O.*  
514 *lenticularis* from Los Roques archipelago in the Caribbean Sea of Venezuela, and they precisely  
515 represented some differences such as the cingulum undulation and the long 2' plate in *O. siamensis*  
516 which are absent in *O. lenticularis* (cf. Figs 14, 16. in Gamboa-Márquez et al. 1994). In spite of  
517 these differences, Faust et al. (1996) surprisingly made a major confusion between the two species  
518 in their taxonomic study and provided mistaken descriptions, perpetuating confusions between these  
519 species (Chomérat et al. 2019a, b). These studies however revealed a great diversity and emphasize  
520 the presence of both *O. siamensis* and *O. lenticularis* in Caribbean samples, which we can confirm  
521 in the present study using molecular data. On the light of this evidence, and since previous studies  
522 showed an absence of toxicity in *O. lenticularis* in contrast with *O. siamensis* (Sato et al., 2011;  
523 Chomérat et al., 2019b, 2020b), several reports of toxic '*O. lenticularis*' from the Caribbean  
524 (Tosteson et al., 1986; Ballantine et al., 1988; Mercado et al., 1994; Meunier et al., 1997; e.g.  
525 Ashton et al., 2003; Pérez-Guzmán et al., 2008) appear now doubtful and need to be reinvestigated.

526 Moreover, descriptions of morphospecies with poor morphological distinctive features have  
527 from the Caribbean added sources of confusions. For instance, the descriptions of *O. labens* (Faust  
528 and Morton, 1995), *O. belizeana*, *O. caribbeana*, and *O. marina* (Faust, 1999) introduced new  
529 names in an existing context of confused taxonomy. Size ranges of these species considerably  
530 overlap with other species and considering large variations observed in populations observed in the  
531 present study, it cannot be excluded that some of these species are junior synonyms of existing taxa,  
532 as aforementioned for *O. labens*, likely a synonym for *O. siamensis*. A similar situation occurs with  
533 *O. marina* which does not seem to be different from *O. lenticularis* except that it has a larger size,  
534 as putatively identified by Irola-Sansores et al. (2018). Molecular data from the present study reveal  
535 that larger specimens with this morphology are genetically identical with *O. lenticularis*, making  
536 the existence of *O. marina* as a separate species in question.

537 Reports of *O. ovata* all over the Caribbean [St. Barthelemy Island Besada et al.(1982);  
538 Virgin Islands, Carlson (1984); Venezuela, Gamboa Márquez et al. (1994); Belize and Puerto Rico,  
539 Faust et al. (1996), Cuba, Delgado et al. (2006)] are based exclusively on morphology.  
540 Nevertheless, recent studies demonstrated that morphology of *O. cf. ovata* is not distinctive and  
541 divergent genotypes such as *O. cf. ovata* complex (Nascimento et al., 2020), *Ostreopsis* sp. 1 (Sato  
542 et al., 2011) or *Ostreopsis* sp. 7 (Tawong et al., 2014) are cryptic. Hence our molecular

543 characterization confirms the presence of a genotype of the *O. cf. ovata* complex in Guadeloupe  
544 Island, but, as it was infrequently found only at Rivière Sens, other genotypes may be present in  
545 other sites. In contrast with larger species such as *O. lenticularis* and *O. siamensis*, this species  
546 received little attention in the Caribbean area, probably because it was less abundant (Carlson,  
547 1984) and it has not been studied thoroughly. Since *O. cf. ovata* is now a widely common species  
548 worldwide, with some strains producing high levels of toxins (e.g. Nascimento et al., 2012;  
549 Tartaglione et al., 2017) causing health concerns and beaches closures (Tester et al., 2020), studies  
550 focussing on its genetics, distribution and potential toxicity should be further addressed in  
551 Guadeloupe Island and more generally in the Caribbean Sea.

552 By contrast, *O. heptagona* has been mentioned several times in the Gulf of Mexico where it  
553 has been originally described (Norris et al., 1985; Bomber et al., 1988, 1989; Okolodkov et al.,  
554 2007, 2014; Aguilar-Trujillo et al., 2017) and in the Caribbean area (Faust et al., 1996; Morton and  
555 Faust, 1997; Almazán-Becerril et al., 2015; Irola-Sansores et al., 2018). The presence of *O.*  
556 *heptagona* in Guadeloupe Island constitutes the southernmost report to date. In spite of its regular  
557 presence in various parts of this area, the potential toxicity of this species remains unclear, and the  
558 limited toxicity to mice assessed with an unclear  $LD_{50} > 5 \times 10^6$  cells·kg<sup>-1</sup> (according to Babinchak  
559 in Norris et al. 1985) needs to be re-evaluated.

560 Species identification is hardly possible by light microscopy due to large variations in size.  
561 Poor distinctive morphological characters lead to considerable confusions in the past and the use of  
562 new identification tools based on molecular data appears to be essential for ecological studies and  
563 monitoring purposes. This work is however essential to generate a reference dataset of sequences,  
564 which constitutes a prerequisite for further development of molecular techniques based on  
565 environmental DNA such as probes for fluorescent *in situ* hybridization assay (Pitz et al., 2021),  
566 RT-PCR assays and metabarcoding analyses. While light microscopic observations can accurately  
567 estimate the abundance of the genus *Ostreopsis* (Boisnoir et al., 2018, 2019, 2020) studying species  
568 distribution, dynamics and phenology will be facilitated by implementation of such tools at the  
569 scale of the Caribbean.

570

### 571 ***Evidence of parasitism on Ostreopsis cells***

572 Parasitoids belonging to the genus *Amoebophrya* are known to infect various planktonic organisms  
573 such as radiolarians or dinoflagellate populations (Cachon, 1964) as *Akashiwo*, *Alexandrium*,  
574 *Ceratium*, *Cochlodinium*, *Dinophysis*, *Gymnodinium*, *Gyrodinium*, *Karlodinium*, *Phalacroma*,  
575 *Prorocentrum*, and *Scrippsiella* (Coats and Park, 2002; Chambouvet et al., 2008; Chambouvet,  
576 2009; Alves-de-Souza et al., 2012). Interestingly, and in spite of being described as a generalist  
577 parasitoid which can infect a great variety of hosts, *Ostreopsis* species have never been associated  
578 with *Amoebophrya* infection, and thus present data constitute the first evidence that such events

579 occur in natural populations. From our data, the same parasitoid species can infect at least two  
580 different *Ostreopsis* species, namely *O. lenticularis* and *O. heptagona*, which confirms a low  
581 specificity. The compact mass within dinoflagellate cells could correspond to the trophont stage, an  
582 advanced stage of the infection caused by the parasitoid *Amoebophrya* (Cachon, 1964; Chambouvet  
583 et al., 2008). In addition, infections of other dinoflagellate genera present in the same samples (e.g.  
584 *Gambierdiscus* spp., *Prorocentrum* spp.) have not been investigated and are possible. From a  
585 molecular point of view, the genotype of the parasitoid found in the present study is rather distant  
586 from *Amoebophrya* strains isolated from other dinoflagellates and only one sequence of this  
587 genotype was already available in GenBank (MK752531, *Amoebophrya* sp. isolate AT5), without  
588 any indication of the putative host and origin.

589 This unexpected finding is an illustration of serendipity, and as it was not the focus of the study,  
590 several aspects regarding parasitism remain in question due to inappropriate sampling. The presence  
591 of *Amoebophrya* infecting populations of *Ostreopsis* spp. could impact their dynamics and  
592 probably constitute an important controlling factor of the blooms (Chambouvet et al., 2008;  
593 Mazzillo et al., 2011; Park et al., 2019). Further analyses should focus on determining the host  
594 specificity, the prevalence/infectivity, and the generation time of *Amoebophrya* sp. (Coats and Park,  
595 2002). As suggested by Kim and Park (2016), parasitism may play a role in the toxicity of  
596 dinoflagellates, and such interactions should probably better taken into consideration in studies of  
597 benthic toxigenic taxa.

598

### 599 **Acknowledgments**

600 The authors extend special to thanks to Dr. Marc Gottshling for his advices regarding phylogenetic  
601 analysis and for sharing his alignment of gonyaulacean dinophytes, and to Dr Philipp Hess for  
602 editing of the English language. Authors acknowledge the support of the Collectivité Territoriale de  
603 Martinique for allowing this project been carried out.

604 AB wishes to express her deep gratitude to the GDR Phycotox and the members of the Club  
605 Soroptimist Diamant Les Rivières. The Regional Council of Brittany, the General Council of  
606 Finistère, the urban community of Concarneau Cornouaille Agglomération and the European  
607 Regional Development Fund (ERDF) are acknowledged for the funding of the Sigma 300 FE-SEM  
608 of the Concarneau Marine Biology Station.

609

### 610 **Disclosure statement**

611 No potential conflict of interest was reported by the authors.

612

613 **Funding**

614 This work is part of CARTAGO project and was supported by funds of the GDR Phycotox (Ifremer  
615 / CNRS 3659 research network on HABs) and the scholarship of Soroptimist-Union française.

616

617 **Authors contributions**

618 A. Boisnoir: original concept, sampling, microscopy, drafting and editing manuscript; G. Bilien:  
619 molecular analysis, sequencing and editing manuscript, R. Lemée: original concept, editing  
620 manuscript; N. Chomérat: original concept, microscopy, analysis of molecular data, drafting and  
621 editing manuscript.

622

623 **References**

- 624 Açaf, L., Abboud-Abi Saab, M., Khoury-Hanna, M., Lemée, R., 2020. Bloom dynamics of the  
625 newly described toxic benthic dinoflagellate *Ostreopsis fattorussoi* along the Lebanese coast  
626 (Eastern Mediterranean). *Reg. Stud. Mar. Sci.* 38, 101338.
- 627 Accoroni, S., Romagnoli, T., Penna, A., Capellacci, S., Ciminiello, P., Dell'Aversano, C.,  
628 Tartaglione, L., Saab, M.A.-A., Giussani, V., Asnaghi, V., Chiantore, M., Totti, C., 2016.  
629 *Ostreopsis fattorussoi* sp. nov. (Dinophyceae), a new benthic toxic *Ostreopsis* species from  
630 the eastern Mediterranean Sea. *J. Phycol.* 52, 1064–1084.
- 631 Accoroni, S., Totti, C., Romagnoli, T., Giulietti, S., Glibert, P.M., 2020. Distribution and potential  
632 toxicity of benthic harmful dinoflagellates in waters of Florida Bay and the Florida Keys.  
633 *Mar. Environ. Res.* 155, 104891.
- 634 Aguilar-Trujillo, A.C., Okolodkov, Y.B., Herrera-Silveira, J.A., Merino-Virgilio, F. del C., Galicia-  
635 García, C., 2017. Taxocoenosis of epibenthic dinoflagellates in the coastal waters of the  
636 northern Yucatan Peninsula before and after the harmful algal bloom event in 2011–2012.  
637 *Mar. Pollut. Bull.* 119, 396–406.
- 638 Alcalá, A.C., Alcalá, L.C., Garth, J.S., Yasumura, D., Yasumoto, T., 1988. Human fatality due to  
639 ingestion of the crab *Demania reynaudii* that contained a palytoxin-like toxin. *Toxicon* 26,  
640 105–107.
- 641 Almazán-Becerril, A., Escobar-Morales, S., Rosiles-González, G., Valadez, F., 2015. Benthic-  
642 epiphytic dinoflagellates from the northern portion of the Mesoamerican Reef System. *Bot.*  
643 *Mar.* 58, 115–128.
- 644 Alves-de-Souza, C., Varela, D., Iriarte, J.L., González, H.E., Guillou, L., 2012. Infection dynamics  
645 of Amoebophryidae parasitoids on harmful dinoflagellates in a southern Chilean fjord  
646 dominated by diatoms. *Aquat. Microb. Ecol.* 66, 183–197.
- 647 Ashton, M., Tosteson, T., Tosteson, C., 2003. The effect of elevated temperature on the toxicity of  
648 the laboratory cultured dinoflagellate *Ostreopsis lenticularis* (Dinophyceae). *Rev. Biol.*  
649 *Trop.* 51, 1–6.
- 650 Ballantine, D.L., Bardales, A.T., Tosteson, C.G., 1985. Seasonal abundance of *Gambierdiscus*  
651 *toxicus* and *Ostreopsis* sp. in coastal waters of southwest Puerto-Rico, in: *Proceeding of the*  
652 *Fifth International Coral Reef Congress*. Tahiti, pp. 417–422.
- 653 Ballantine, D.L., Tosteson, T.R., Bardales, A.T., 1988. Population dynamics and toxicity of natural  
654 populations of benthic dinoflagellates in southwestern Puerto Rico. *J. Exp. Mar. Biol. Ecol.*  
655 119, 201–212.

- 656 Berland, B., Grzebyk, D., Thomassin, B., 1992. Benthic dinoflagellates from the coral reef lagoon  
657 of Mayotte Island (S-W Indian Ocean); identification, toxicity and preliminary  
658 ecophysiological study. *Bull. Société Pathol. Exot.* 1990 85, 453–6.
- 659 Besada, E.G., Loeblich, L.A., Loeblich III, A.R., 1982. Observations on tropical, benthic  
660 dinoflagellates from ciguatera-endemic areas: *Coolia*, *Gambierdiscus*, and *Ostreopsis*. *Bull.*  
661 *Mar. Sci.* 32, 723–735.
- 662 Biré, R., Trottereau, S., Lemée, R., Delpont, C., Chabot, B., Aumond, Y., Krys, S., 2013. Occurrence  
663 of palytoxins in marine organisms from different trophic levels of the French Mediterranean  
664 coast harvested in 2009. *Harmful Algae* 28, 10–22.
- 665 Biré, R., Trottereau, S., Lemée, R., Oregioni, D., Delpont, C., Krys, S., Guérin, T., 2015. Hunt for  
666 palytoxins in a wide variety of marine organisms harvested in 2010 on the French  
667 Mediterranean coast. *Mar. Drugs* 13, 5425–5446.
- 668 Boisnoir, A., Pascal, P.-Y., Cordonnier, S., Lemée, R., 2018. Depth distribution of benthic  
669 dinoflagellates in the Caribbean Sea. *J. Sea Res.* 135, 74–83.
- 670 Boisnoir, A., Pascal, P.-Y., Cordonnier, S., Lemée, R., 2019. Spatio-temporal dynamics and biotic  
671 substrate preferences of benthic dinoflagellates in the Lesser Antilles, Caribbean sea.  
672 *Harmful Algae* 81, 18–29.
- 673 Boisnoir, A., Pascal, P.-Y., Chomérat, N., Lemée, R., 2020. Distribution of potentially toxic  
674 epiphytic dinoflagellates in Saint Martin Island (Caribbean Sea, Lesser Antilles).  
675 *Cryptogam. Algol.* 41, 47–54.
- 676 Bomber, J.W., Morton, S.L., Babinchak, J.A., Norris, D.R., Morton, J.G., 1988. Epiphytic  
677 dinoflagellates of drift algae — another toxigenic community in the Ciguatera Food Chain.  
678 *Bull. Mar. Sci.* 43, 204–214.
- 679 Bomber, J.W., Rubio, M.G., Norris, D.R., 1989. Epiphytism of dinoflagellates associated with the  
680 disease ciguatera: substrate specificity and nutrition. *Phycologia* 28, 360–368.
- 681 Borsato, G.T., Salgueiro, F., da Silva, C.G.T., Menezes-Salgueiro, A.D., Nascimento, S.M., 2020.  
682 *Ostreopsis lenticularis* Y. Fukuyo (Dinophyceae, Gonyaulacales) from the South Atlantic  
683 Ocean: morphological and molecular characterization. *Mar. Pollut. Bull.* 158, 111441.
- 684 Cachon, J., 1964. Contribution à l'étude des péridiniens parasites : Cytologie, cycles évolutifs. *Ann.*  
685 *Sci. Nat. Zool. Biol. Anim. Serie* 12, 1–158, pl. 1–36.
- 686 Carlson, R.D., 1984. Distribution, periodicity, and culture of benthic/epiphytic dinoflagellates in a  
687 ciguatera endemic region of the Caribbean. PhD Thesis. Southern Illinois University,  
688 Carbondale.
- 689 Carlson, R.D., Tindall, D.R., 1985. Distribution and periodicity of toxic dinoflagellates in the Virgin  
690 Islands., in: *Proceeding of the Third International Conference on Toxic Dinoflagellates.*  
691 Presented at the Toxic dinoflagellates, Anderson, DM, White, AW, Baden, DG (eds), pp.  
692 171–176.
- 693 Carnicer, O., Tunin-Ley, A., Andree, K.B., Turquet, J., Diogène, J., Fernández-Tejedor, M., 2015.  
694 Contribution to the genus *Ostreopsis* in Reunion Island (Indian Ocean): molecular,  
695 morphologic and toxicity characterization. *Cryptogam. Algol.* 36, 101–119.
- 696 Chambouvet, A., Morin, P., Marie, D., Guillou, L., 2008. Control of toxic marine dinoflagellate  
697 blooms by serial parasitic killers. *Science* 322, 1254–1257.
- 698 Chambouvet, A., 2009. Les amoebophryidae (Syndiniales) parasitoïdes de dinoflagellés : cycle de  
699 vie, dynamique et spécificité in situ. *Parasitologie.* PhD thesis. Paris 6, France.
- 700 Chesnick, J.M., Cox, E.R., 1985. Thecal plate tabulation and variation in *Peridinium balticum*  
701 (Pyrrhophyta: Peridinales). *Trans. Am. Microsc. Soc.* 104, 387–394.
- 702 Chomérat, N., Couté, A., 2008. *Protoperidinium bolmonense* sp. nov. (Peridinales, Dinophyceae), a  
703 small dinoflagellate from a brackish hypereutrophic lagoon (South of France). *Phycologia*  
704 47, 392–403.
- 705 Chomérat, N., Bilien, G., Zentz, F., 2019a. A taxonomical study of benthic *Prorocentrum* species  
706 (Prorocentrales, Dinophyceae) from Anse Dufour (Martinique Island, eastern Caribbean  
707 Sea). *Mar. Biodivers.* 49, 1299–1319.
- 708 Chomérat, N., Bilien, G., Derrien, A., Henry, K., Ung, A., Viallon, J., Darius, H.T., Mahana iti Gatti,  
709 C., Roué, M., Hervé, F., Réveillon, D., Amzil, Z., Chinain, M., 2019b. *Ostreopsis*

- 710 *lenticularis* Y. Fukuyo (Dinophyceae, Gonyaulacales) from French Polynesia (South Pacific  
711 Ocean): A revisit of its morphology, molecular phylogeny and toxicity. *Harmful Algae* 84,  
712 95–111.
- 713 Chomérat, N., Bilien, G., Couté, A., Quod, J.-P., 2020a. Reinvestigation of *Ostreopsis*  
714 *mascarenensis* Quod (Dinophyceae, Gonyaulacales) from Réunion Island (SW Indian  
715 Ocean): molecular phylogeny and emended description. *Phycologia* 59, 140–153.
- 716 Chomérat, N., Bilien, G., Viallon, J., Hervé, F., Réveillon, D., Henry, K., Zubia, M., Vieira, C., Ung,  
717 A., Gatti, C.M. iti, Roué, M., Derrien, A., Amzil, Z., Darius, H.T., Chinain, M., 2020b.  
718 Taxonomy and toxicity of a bloom-forming *Ostreopsis* species (Dinophyceae,  
719 Gonyaulacales) in Tahiti island (South Pacific Ocean): one step further towards resolving  
720 the identity of *O. siamensis*. *Harmful Algae* 98, 101888.
- 721 Coats, D.W., Park, M.G., 2002. Parasitism of photosynthetic dinoflagellates by three strains of  
722 *Amoebophrya* (dinophyta): parasite survival, infectivity, generation time, and host  
723 specificity. *J. Phycol.* 38, 520–528.
- 724 Cohu, S., Mangialajo, L., Thibaut, T., Blanfuné, A., Marro, S., Lemée, R., 2013. Proliferation of the  
725 toxic dinoflagellate *Ostreopsis* cf. *ovata* in relation to depth, biotic substrate and  
726 environmental factors in the North West Mediterranean Sea. *Harmful Algae* 24, 32–44.
- 727 Darriba, D., Taboada, G.L., Doallo, R., Posada, D., 2012. jModelTest 2: more models, new  
728 heuristics and parallel computing. *Nat. Methods* 9, 772–772.
- 729 Delgado, G., Lechuga-Devéze, C.H., Popowski, G., Troccoli, L., Salinas, C.A., 2006. Epiphytic  
730 dinoflagellates associated with ciguatera in the northwestern coast of Cuba. *Rev. Biol. Trop.*  
731 54, 299–310.
- 732 Durando, P., Ansaldi, F., Oreste, P., Moscatelli, P., Marensi, L., Grillo, C., Gasparini, R., Icardi, G.,  
733 2007. *Ostreopsis ovata* and human health: Epidemiological and clinical features of  
734 respiratory syndrome outbreaks from a two year syndromic surveillance, 2005–2006, in  
735 northwest Italy. *Eur. Commun. Dis. Bull.* 12, E070607.1.
- 736 Edgar, R., 2004. MUSCLE: a multiple sequence alignment method with reduced time and space  
737 complexity. *BMC Bioinformatics* 5, 113.
- 738 Faust, M.A., 1995. Observation of sand-dwelling toxic dinoflagellates (dinophyceae) from widely  
739 differing sites, including two new species. *J. Phycol.* 31, 996–1003.
- 740 Faust, M.A., Morton, S.L., 1995. Morphology and ecology of the marine dinoflagellate *Ostreopsis*  
741 *labens* sp. nov. (dinophyceae). *J. Phycol.* 31, 456–463.
- 742 Faust, M.A., Gullledge, R.A., 1996. Associations of microalgae and meiofauna in floating detritus at  
743 a mangrove island, Twin Cays, Belize. *J. Exp. Mar. Biol. Ecol.* 197, 159–175.
- 744 Faust, M.A., Morton, S.L., Quod, J.P., 1996. Further SEM study of marine dinoflagellates: The  
745 genus *Ostreopsis* (Dinophyceae). *J. Phycol.* 32, 1053–1065.
- 746 Faust, M.A., 1999. Three new *Ostreopsis* species (Dinophyceae): *O. marinus* sp. nov., *O. belizeanus*  
747 sp. nov., and *O. caribbeanus* sp. nov. *Phycologia* 38, 92–99.
- 748 Faust, M.A., 2004. The dinoflagellates of Twin Cays, Belize: biodiversity, distribution and  
749 vulnerability. *Atoll Res. Bull.* 514, 1–20.
- 750 Fukuyo, Y., 1981. Taxonomical study on benthic dinoflagellates collected in coral reefs. *Bull. Jpn.*  
751 *Soc. Sci. Fish.* 47, 967–978.
- 752 Gallitelli, M., Ungaro, N., Addante, L.M., Procacci, V., Silver, N.G., Sabbà, C., 2005. Respiratory  
753 illness as a reaction to tropical algal blooms occurring in a temperate climate. *J. Am. Med.*  
754 *Assoc.* 293, 2595–2600.
- 755 Gamboa-Márquez, J., Sánchez Suárez, I., La Barbera Sánchez, A., 1994. Dinoflagelados  
756 (Pyrrhophyta) del archipiélago Los Roques (Venezuela): familias Proocentraceae y  
757 *Ostreopsidaceae*. *Acta Científica Venez.* 45, 140–52.
- 758 Gouy, M., Guindon, S., Gascuel, O., 2010. SeaView version 4: A multiplatform graphical user  
759 interface for sequence alignment and phylogenetic tree building. *Mol. Biol. Evol.* 27, 221–  
760 224.
- 761 Guindon, S., Dufayard, J.-F., Lefort, V., Anisimova, M., Hordijk, W., Gascuel, O., 2010. New  
762 algorithms and methods to estimate maximum-likelihood phylogenies: assessing the  
763 performance of PhyML 3.0. *Syst. Biol.* 59, 307–321.

- 764 Guiry, M.D., Guiry, G.M., 2021. *Algaebase*. World-wide electronic publication, National University  
765 of Ireland, Galway. <http://www.algaebase.org>; searched on 04 February 2021. [WWW  
766 Document]. URL (accessed 2.4.21).
- 767 Hoppenrath, M., Murray, S., Chomérat, N., Horiguchi, T., 2014. Marine benthic dinoflagellates -  
768 unveiling their worldwide biodiversity, Schweizerbart'sche Verlagbuchhandlung. ed. Kleine  
769 Senckenberg-Reihe, Germany.
- 770 Irola-Sansores, E.D., Delgado-Pech, B., García-Mendoza, E., Núñez-Vázquez, E.J., Olivos-Ortiz,  
771 A., Almazán-Becerril, A., 2018. Population dynamics of benthic-epiphytic dinoflagellates on  
772 two macroalgae from coral reef systems of the Northern Mexican Caribbean. *Front. Mar.*  
773 *Sci.* 5, 487.
- 774 Jauzein, C., Açaf, L., Accoroni, S., Asnaghi, V., Fricke, A., Hachani, M.A., Abboud-Abi Saab, M.,  
775 Chiantore, M., Mangialajo, L., Totti, C., Zaghmouri, I., Lemée, R., 2018. Optimization of  
776 sampling, cell collection and counting for the monitoring of benthic harmful algal blooms:  
777 Application to *Ostreopsis* spp. blooms in the Mediterranean Sea. *Ecol. Indic.* 91, 116–127.
- 778 Junqueira de Azevedo Tibiriçá, C.E.J.A., Leite, I.P., Batista, T.V.V., Fernandes, L.F., Chomérat, N.,  
779 Hervé, F., Hess, P., Mafra, L.L., 2019. *Ostreopsis* cf. *ovata* bloom in Currais, Brazil:  
780 phylogeny, toxin profile and contamination of mussels and marine plastic litter. *Toxins* 11,  
781 446.
- 782 Katikou, P., 2007. Chemistry of Palytoxins and Ostreocins, in: Botana, L.M. (Ed.), *Phycotoxins:*  
783 *Chemistry and Biochemistry*. Blackwell Publishing, Ames, Iowa, USA, pp. 75–93.
- 784 Katoh, K., Standley, D.M., 2013. MAFFT Multiple sequence alignment software version 7:  
785 Improvements in performance and usability. *Mol. Biol. Evol.* 30, 772–780.
- 786 Kim, S., Park, M.G., 2016. Effect of the endoparasite *Amoebophrya* sp. on toxin content and  
787 composition in the paralytic shellfish poisoning dinoflagellate *Alexandrium fundyense*  
788 (Dinophyceae). *Harmful Algae* 51, 10–15.
- 789 Kumar, S., Stecher, G., Li, M., Knyaz, C., Tamura, K., 2018. MEGA X: Molecular evolutionary  
790 genetics analysis across computing platforms. *Mol. Biol. Evol.* 35, 1547–1549.
- 791 Lee, B., Park, M.G., 2020. Distribution and genetic diversity of the toxic benthic dinoflagellate  
792 genus *Ostreopsis* in Korea. *Harmful Algae* 96, 101820.
- 793 Mazzillo, F.F.M., Ryan, J.P., Silver, M.W., 2011. Parasitism as a biological control agent of  
794 dinoflagellate blooms in the California Current System. *Harmful Algae* 10, 763–773.
- 795 Mercado, J.A., Rivera-Rentas, A.L., Gonzalez, I., Tosteson, T.R., Molgó, J., Motta, G., 1994.  
796 Neuro- and myo-toxicity of extracts from the benthic dinoflagellate *Ostreopsis lenticularis* is  
797 sensitive to  $\mu$ -conotoxin. *Soc. Neurosci. Abstr.* 20, 1224–1230.
- 798 Meunier, F.A., Mercado, J.A., Molgó, J., Tosteson, T.R., Escalona de Motta, G., 1997. Selective  
799 depolarization of the muscle membrane in frog nerve-muscle preparations by a  
800 chromatographically purified extract of the dinoflagellate *Ostreopsis lenticularis*. *Br. J.*  
801 *Pharmacol.* 121, 1224–1230.
- 802 Morton, S.L., Faust, M.A., 1997. Survey of toxic epiphytic dinoflagellates from the Belizean  
803 Barrier Reef Ecosystem. *Bull. Mar. Sci.* 61, 899–906.
- 804 Nascimento, S.M., Corrêa, E.V., Menezes, M., Varela, D., Paredes, J., Morris, S., 2012. Growth and  
805 toxin profile of *Ostreopsis* cf. *ovata* (Dinophyta) from Rio de Janeiro, Brazil. *Harmful Algae*  
806 13, 1–9.
- 807 Nascimento, S.M., Neves, R.A.F., De'Carli, G.A.L., Borsato, G.T., da Silva, R.A.F., Melo, G.A., de  
808 Morais, A.M., Cockell, T.C., Fraga, S., Menezes-Salgueiro, A.D., Mafra, L.L., Hess, P.,  
809 Salgueiro, F., 2020. *Ostreopsis* cf. *ovata* (Dinophyceae) molecular phylogeny, morphology,  
810 and detection of ovatoxins in strains and field samples from Brazil. *Toxins* 12, 70.
- 811 Nguyen-Ngoc, L., Doan-Nhu, H., Larsen, J., Phan-Tan, L., Nguyen, X.-V., Lundholm, N., Chu,  
812 T.V., Huynh-Thi, D.N., 2021. Morphological and genetic analyses of *Ostreopsis*  
813 (Dinophyceae, Gonyaulacales, Ostreopsidaceae) species from Vietnamese waters with a re-  
814 description of the type species, *O. siamensis*. *J. Phycol.*
- 815 Ninčević Gladan, Ž., Arapov, J., Casabianca, S., Penna, A., Honsell, G., Brovedani, V., Pelin, M.,  
816 Tartaglione, L., Sosa, S., Dell'Aversano, C., Tubaro, A., Žuljević, A., Grbec, B., Čavar, M.,

- 817 Bužančić, M., Bakrač, A., Skejić, S., 2019. Massive occurrence of the harmful benthic  
818 dinoflagellate *Ostreopsis* cf. *ovata* in the Eastern Adriatic Sea. *Toxins* 11, 300.
- 819 Norris, D.R., Bomber, J.W., Balech, E., 1985. Benthic dinoflagellates associated with ciguatera  
820 from the Florida Keys. I. *Ostreopsis heptagona* sp. nov., in: *Toxic Dinoflagellates*. D.M.  
821 Anderson, A.W. White & D.G. Baden, pp. 39–44.
- 822 Okolodkov, Y.B., Campos-Bautista, G., Gárate-Lizárraga, I., González-González, J.A.G.,  
823 Hoppenrath, M., Arenas, V., 2007. Seasonal changes of benthic and epiphytic dinoflagellates  
824 in the Veracruz reef zone, Gulf of Mexico. *Aquat. Microb. Ecol.* 47, 223–237.
- 825 Okolodkov, Y.B., Merino-Virgilio, F. del C., Aké-Castillo, J.A., Aguilar-Trujillo, A.C., Espinosa-  
826 Matías, S., Herrera-Silveira, J.A., 2014. Seasonal changes in epiphytic dinoflagellate  
827 assemblages near the northern coast of the Yucatan Peninsula, Gulf of Mexico. *Acta Bot.*  
828 *Mex.* 107, 121–151.
- 829 Onuma, Y., Satake, M., Ukena, T., Roux, J., Chanteau, S., Rasolofonirina, N., Ratsimaloto, M.,  
830 Naoki, H., Yasumoto, T., 1999. Identification of putative palytoxin as the cause of  
831 clupeotoxism. *Toxicon* 37, 55–65.
- 832 Park, B.S., Kim, S., Kim, J.-H., Ho Kim, J., Han, M.-S., 2019. Dynamics of *Amoebophrya* parasites  
833 during recurrent blooms of the ichthyotoxic dinoflagellate *Cochlodinium polykrikoides* in  
834 Korean coastal waters. *Harmful Algae* 84, 119–126.
- 835 Park, J., Hwang, J., Hyung, J.-H., Yoon, E.Y., 2020. Temporal and spatial distribution of the toxic  
836 epiphytic dinoflagellate *Ostreopsis* cf. *ovata* in the Coastal Waters off Jeju Island, Korea.  
837 *Sustainability* 12, 5864.
- 838 Parsons, M.L., Aligizaki, K., Bottein, M.-Y.D., Fraga, S., Morton, S.L., Penna, A., Rhodes, L.,  
839 2012. *Gambierdiscus* and *Ostreopsis*: Reassessment of the state of knowledge of their  
840 taxonomy, geography, ecophysiology, and toxicology. *Harmful Algae*, *Harmful Algae--The*  
841 *requirement for species-specific information* 14, 107–129.
- 842 Penna, A., Fraga, S., Battocchi, C., Casabianca, S., Giacobbe, M.G., Riobó, P., Vernesi, C., 2010. A  
843 phylogeographical study of the toxic benthic dinoflagellate genus *Ostreopsis* Schmidt. *J.*  
844 *Biogeogr.* 37, 830–841.
- 845 Pérez-Guzmán, L., Pérez-Matos, A.E., Rosado, W., Tosteson, T.R., Govind, N.S., 2008. Bacteria  
846 associated with toxic clonal cultures of the dinoflagellate *Ostreopsis lenticularis*. *Mar.*  
847 *Biotechnol.* 10, 492–496.
- 848 Pitz, K.J., Richlen, M.L., Fachon, E., Smith, T.B., Parsons, M.L., Anderson, D.M., 2021.  
849 Development of fluorescence in situ hybridization (FISH) probes to detect and enumerate  
850 *Gambierdiscus* species. *Harmful Algae* 101, 101914.
- 851 Quod, J.-P., 1994. *Ostreopsis mascarenensis* sp. nov. (Dinophyceae) dinoflagellé toxique associé à la  
852 ciguatera dans l’Océan Indien. *Cryptogam. Algal.* 243–252.
- 853 Randall, J.E., 2005. Review of clupeotoxism, an often fatal illness from the consumption of  
854 clupeoid fishes. *Pac. Sci.* 59, 73–77.
- 855 Rasband, W.S., 1997. ImageJ. Bethesda, National Institutes of Health, Maryland.
- 856 Rhodes, L.L., Smith, K.F., Murray, J.S., Nishimura, T., Finch, S.C., 2020. Ciguatera fish poisoning:  
857 The risk from an Aotearoa/New Zealand perspective. *Toxins* 12, 50.
- 858 Ronquist, F., Huelsenbeck, J.P., 2003. MrBayes 3: Bayesian phylogenetic inference under mixed  
859 models. *Bioinformatics* 19, 1572–1574.
- 860 Sato, S., Nishimura, T., Uehara, K., Sakanari, H., Tawong, W., Hariganeya, N., Smith, K., Rhodes,  
861 L., Yasumoto, T., Taira, Y., Suda, S., Yamaguchi, H., Adachi, M., 2011. Phylogeography of  
862 *Ostreopsis* along West Pacific coast, with special reference to a novel clade from Japan. *Plos*  
863 *One* 6, e27983.
- 864 Schmidt, J., 1901. Flora of Koh Chang. Contributions to the knowledge of the vegetation in the  
865 Gulf of Siam. Part IV. Peridinales. *J. Bot.* 24, 212–221.
- 866 Shah, M.M.R., An, S.-J., Lee, J.-B., 2014. Occurrence of sand-dwelling and epiphytic  
867 dinoflagellates including potentially toxic species along the coast of Jeju island, Korea. *J.*  
868 *Fish. Aquat. Sci.* 9, 141–156.

- 869 Shears, N.T., Ross, P.M., 2009. Blooms of benthic dinoflagellates of the genus *Ostreopsis*; an  
870 increasing and ecologically important phenomenon on temperate reefs in New Zealand and  
871 worldwide. *Harmful Algae* 8, 916–925.
- 872 Tartaglione, L., Dello Iacovo, E., Mazzeo, A., Casabianca, S., Ciminiello, P., Penna, A.,  
873 Dell’Aversano, C., 2017. Variability in toxin profiles of the Mediterranean *Ostreopsis* cf.  
874 *ovata* and in structural features of the produced Ovatoxins. *Environ. Sci. Technol.* 51,  
875 13920–13928.
- 876 Tawong, W., Nishimura, T., Sakanari, H., Sato, S., Yamaguchi, H., Adachi, M., 2014. Distribution  
877 and molecular phylogeny of the dinoflagellate genus *Ostreopsis* in Thailand. *Harmful Algae*  
878 37, 160–171.
- 879 Tester, P.A., Litaker, R.W., Berdalet, E., 2020. Climate change and harmful benthic microalgae.  
880 *Harmful Algae* 91, 101655.
- 881 Tichadou, L., Glaizal, M., Armengaud, A., Grosseil, H., Lemée, R., Kantin, R., Lasalle, J.-L.,  
882 Drouet, G., Rambaud, L., Malfait, P., de Haro, L., 2010. Health impact of unicellular algae  
883 of the *Ostreopsis* genus blooms in the Mediterranean Sea: experience of the French  
884 Mediterranean coast surveillance network from 2006 to 2009. *Clin. Toxicol. Phila. Pa* 48,  
885 839–844.
- 886 Tillmann, U., Bantle, A., Krock, B., Elbrächter, M., Gottschling, M., 2021. Recommendations for  
887 epitypification of dinophytes exemplified by *Lingulodinium polyedra* and molecular  
888 phylogenetics of the Gonyaulacales based on curated rRNA sequence data. *Harmful Algae*  
889 104, 101956.
- 890 Tindall, D.R., Miller, D.M., Tindall, P.M., 1990. Toxicity of *Ostreopsis lenticularis* from the British  
891 and United States Virgin Islands., in: *Proceedings of the Fourth International Conference on*  
892 *Toxic Marine Phytoplankton*. Presented at the Toxic Marine Phytoplankton, Lund, Sweden,  
893 pp. 424–429.
- 894 Tosteson, T.R., Ballantine, D.L., Tosteson, C.G., Bardales, A.T., Dust, H.D., Higert, T.B., 1986.  
895 Comparative toxicity of *Gambierdiscus toxicus*, *Ostreopsis* cf. *lenticularis* and associated  
896 microflora. *Mar. Fish. Rev.* 48, 57–59.
- 897 Tosteson, T.R., Ballantine, D.L., Tosteson, C.G., Hensley, V., Bardales, A.T., 1989. Associated  
898 bacterial flora, growth, and toxicity of cultured benthic dinoflagellates *Ostreopsis*  
899 *lenticularis* and *Gambierdiscus toxicus*. *Appl. Environ. Microbiol.* 55, 137–141.
- 900 Verma, A., Hoppenrath, M., Dorantes-Aranda, J.J., Harwood, D.T., Murray, S.A., 2016. Molecular  
901 and phylogenetic characterization of *Ostreopsis* (Dinophyceae) and the description of a new  
902 species, *Ostreopsis rhodesae* sp. nov., from a subtropical Australian lagoon. *Harmful Algae*  
903 60, 116–130.
- 904 Vila, M., Abós-Herràndiz, R., Isern-Fontanet, J., Alvarez, J., Berdalet, E., 2016. Establishing the  
905 link between *Ostreopsis* cf. *ovata* blooms and human health impacts using ecology and  
906 epidemiology. *Sci. Mar.* 80, 107–115.
- 907 Zhang, H., Lu, S., Li, Y., Cen, J., Wang, H., Li, Q., Nie, X., 2018. Morphology and molecular  
908 phylogeny of *Ostreopsis* cf. *ovata* and *O. lenticularis* (Dinophyceae) from Hainan Island,  
909 South China Sea. *Phycol. Res.* 66, 3–14.
- 910

911 **Figure legends**

912 **Fig. 1.** Maps showing the location of Guadeloupe Island in the Caribbean Sea and sampling sites  
913

914 **Fig. 2.** Size ranges observed for the four different morphotypes calculated using all available data  
915 from LM and SEM. Crosshairs show the minimum, maximum and mean (at intersection) values for  
916 depth (i.e. DV length) and width. Individual symbols correspond to single-cells used in the  
917 phylogenetic analysis (isolate numbers given in italics) and measured from LM.

918

919 **Figs 3.A–M** SEM micrographs of morphotype 1 (*O. cf. ovata*) from Rivière-Sens (**A–G**) and  
920 morphotype 2 (*O. lenticularis*) from Chapelle (**H–M**). **A:** Apical view. **B:** Antapical view. **C:** Detail  
921 of 2' and 3' plates and apical pore complex (APC). **D:** Left latero-apical view. **E:** Right lateral view  
922 showing the straight cingulum. **F–G:** Detail of thecal pores, with some small pores (arrows) visible.  
923 **H:** Apical view. **I:** Antapical view. **J:** Detail of 2' (short) and 3' plates and apical pore complex  
924 (APC). **K:** Left lateral view showing the straight cingulum. **L:** Right lateral view showing the  
925 straight cingulum. **M:** Detail of the smooth thecal surface with thecal pores of two sizes classes.  
926 Bars: 10 µm (**A–B, H–I, K–L**); 5 µm (**D–E**); 2 µm (**C, J**), 1 µm (**F, M**); 200 nm (**G**).

927

928 **Figs 4. A–I** SEM micrographs of morphotype 3 (*O. siamensis*) from Rivière-Sens. **A:** Apical view.  
929 **B:** Antapical view. **C:** Detail of 2' and 3' plates and apical pore complex (APC). **D:** Ventral view. **E:**  
930 Right lateral view showing the undulated cingulum. **F:** Oblique antapical view showing the strong  
931 undulation of a cell. **G:** Oblique apical view showing the cell undulation and depression of the  
932 hyptheca. **H:** Detail of the ventral area with the 'ventral opening' (Vo) and sulcal plates visible. **I:**  
933 Detail of cell surface with two kinds of thecal pores visible, the smaller indicated with arrows.  
934 Bars, 10 µm (**A–B, D–G**); 5 µm (**C**); 2 µm (**H**); 1 µm (**I**).

935

936 **Figs 5A–H** SEM micrographs of morphotype 4 (*O. heptagona*) from Chapelle site. **A:** Apical view  
937 with the suture 1'/5'' highlighted (arrowhead). **B:** Antapical view. **C:** Detail of the seven-sided first  
938 apical plate 1', note the sutures 1'/5'' (white arrowhead) and 5''/6'' (black arrowhead). **D:** Detail of  
939 the apical pore complex (APC) and long 2' plate contacting 4'' plate. **E:** Left lateral view of a  
940 specimen showing the almost straight and narrow cingulum. **F:** Ventro-apical view. **G:** Detail of the  
941 sulcal area with the ventral opening (Vo) and three sulcal plates visible. **H:** Detail of cell surface  
942 with one type of thecal pores. Bars: 10 µm (**A–B, E–F**); 5 µm (**C**); 2 µm (**D–G**); 1 µm (**H**).

943

944 **Figs 6.A–I** Light micrographs of dissected cells and sulcal plates of morphotype 4 (*O. heptagona*)  
945 from Chapelle **A:** Apical view of an epitheca showing the peculiar shape of 1' plate. **B:** Detail of Po

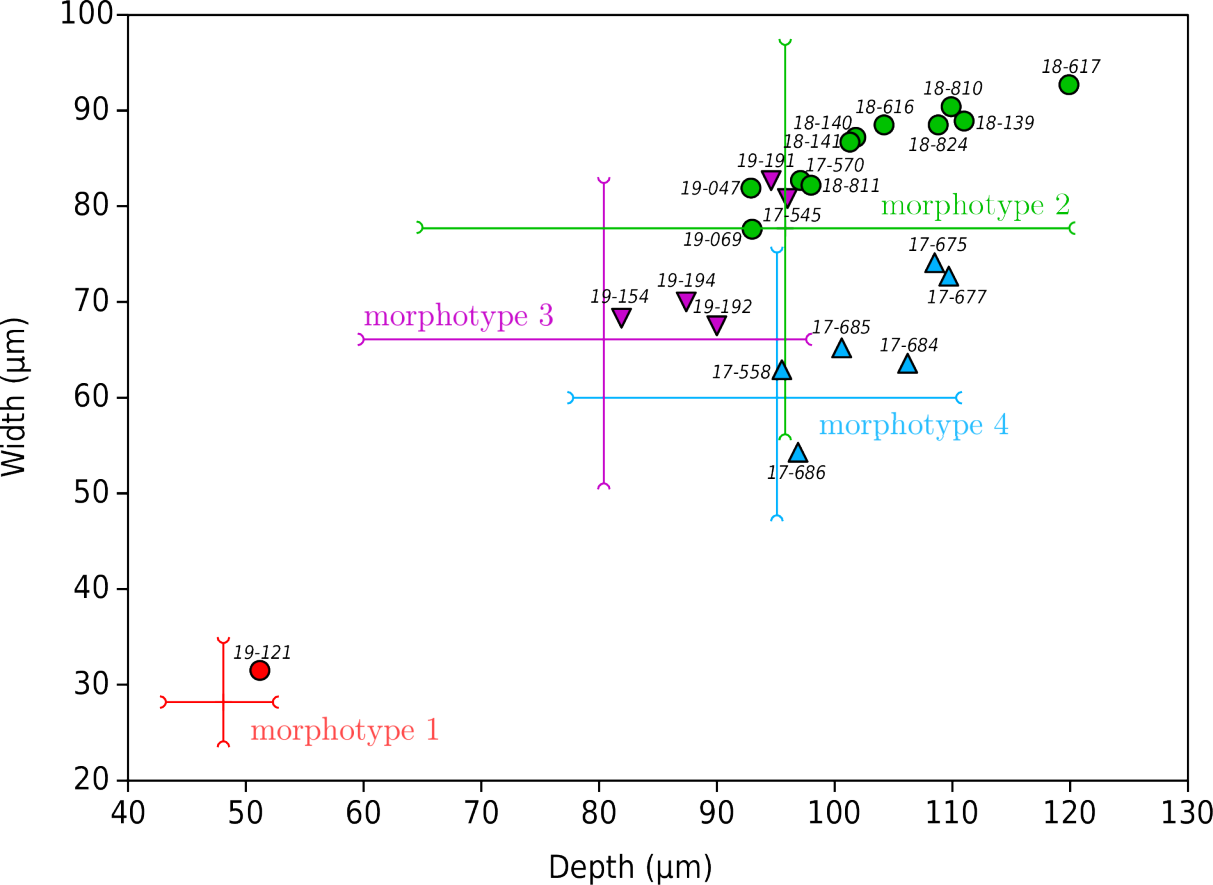
946 and 2' plates. **C:** Detached sulcal area from a broken theca. **D–E:** Views of a sulcal area with  
947 different level of focus, showing some small plates Sp, Sdp and the complex three dimensional  
948 shape of Ssa and Sda. **F:** Detail of an isolated Sp (with a hyaline area) and 1'''. **G:** Detail of the 't'  
949 plate at the left end of Ssa. **H:** Isolated Ssa, Sda bearing a conspicuous list, and Ssp. **I:** Isolated Ssa  
950 and Sda with a detached annular platelet (Sa) encircling Vo. Bars: 20 µm (**A**); 10 µm (**C**); 5 µm (**B**,  
951 **D–I**).

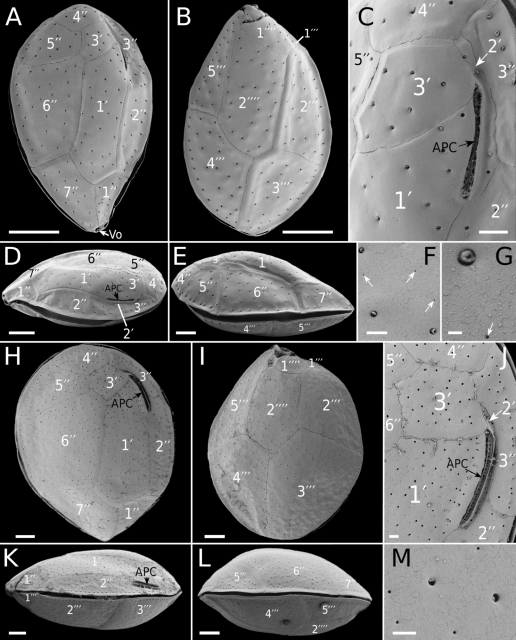
952  
953 **Figs 7.A–O.** Light micrographs of *Ostreopsis* cells with different morphologies used for single-cell  
954 PCR analyses. Codes of each isolate (IFR-) and origin sample (see Table 1) are given in the lower  
955 left corner. **A:** Morphotype 1 (*O. cf. ovata*); **B–E:** Morphotype 2 (*O. lenticularis*); **F–J:**  
956 Morphotype 3 (*O. siamensis*); **K–O:** Morphotype 4 (*O. heptagona*), note that specimen IFR17-685  
957 (**N**) was infected by *Amoebophrya* sp. Bars = 20 µm.

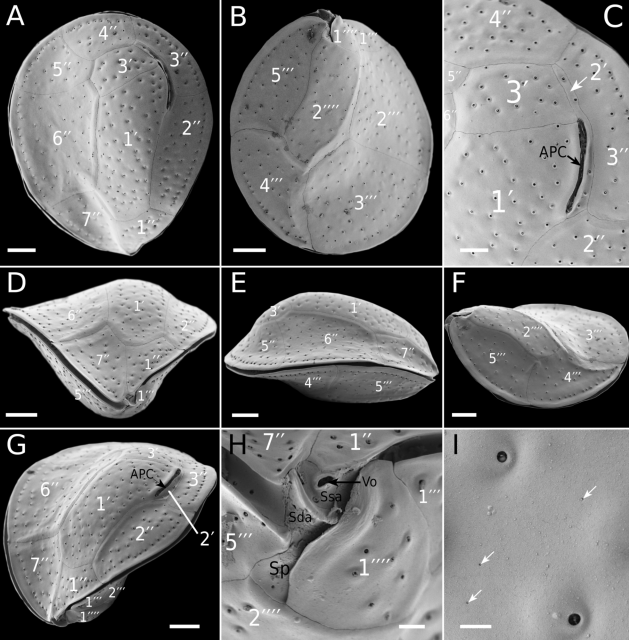
958  
959 **Fig. 8.** Maximum-Likelihood phylogenetic tree based on 189 concatenated sequences of ribosomal  
960 operon (SSU + ITS + LSU D1-D3 and D8-D10) (6382 aligned characters) of different strains of  
961 *Ostreopsidoideae* and other gonyaulaceans as outgroup. *Alexandrium/Centrodinium* subclades are  
962 collapsed for readability (Full tree in supplementary figure S2). Sequences acquired in the present  
963 study are indicated in bold type. Branch robustness was indicated by bootstrap values (ML) and  
964 posterior probabilities (BI). Bootstraps values below 65 and posterior probabilities below 0.9 are  
965 shown with '-'. On the right, vertical bars delimit major clades corresponding to the different  
966 species/genotypes.

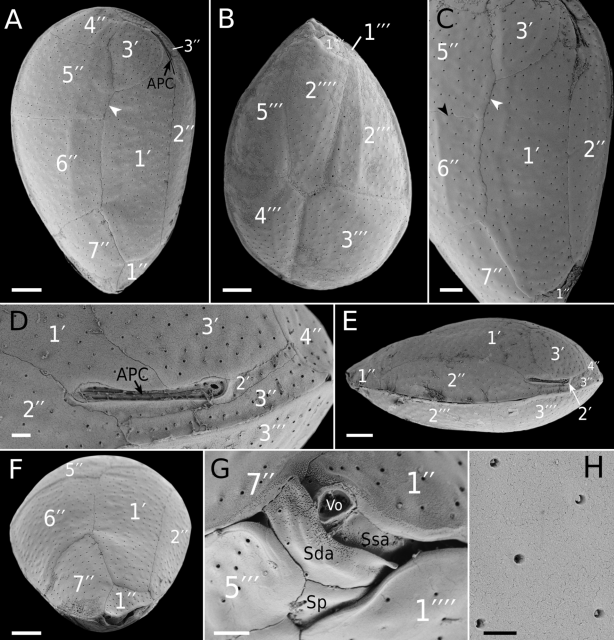
967  
968 **Figs 9 A–F** Light micrographs of Lugol-fixed *Ostreopsis* cells infected by the parasitoid  
969 *Amoebophrya* sp. **A–D:** Cells of *O. lenticularis*, note that three specimens have been used for  
970 sequencing the parasitoid (isolate codes indicated in the lower left corner). **E–F:** Cells of *O.*  
971 *heptagona*. The white arrowheads show the more or less developed trophont stage of *Amoebophrya*  
972 within *Ostreopsis* cells. Bars = 10 µm.

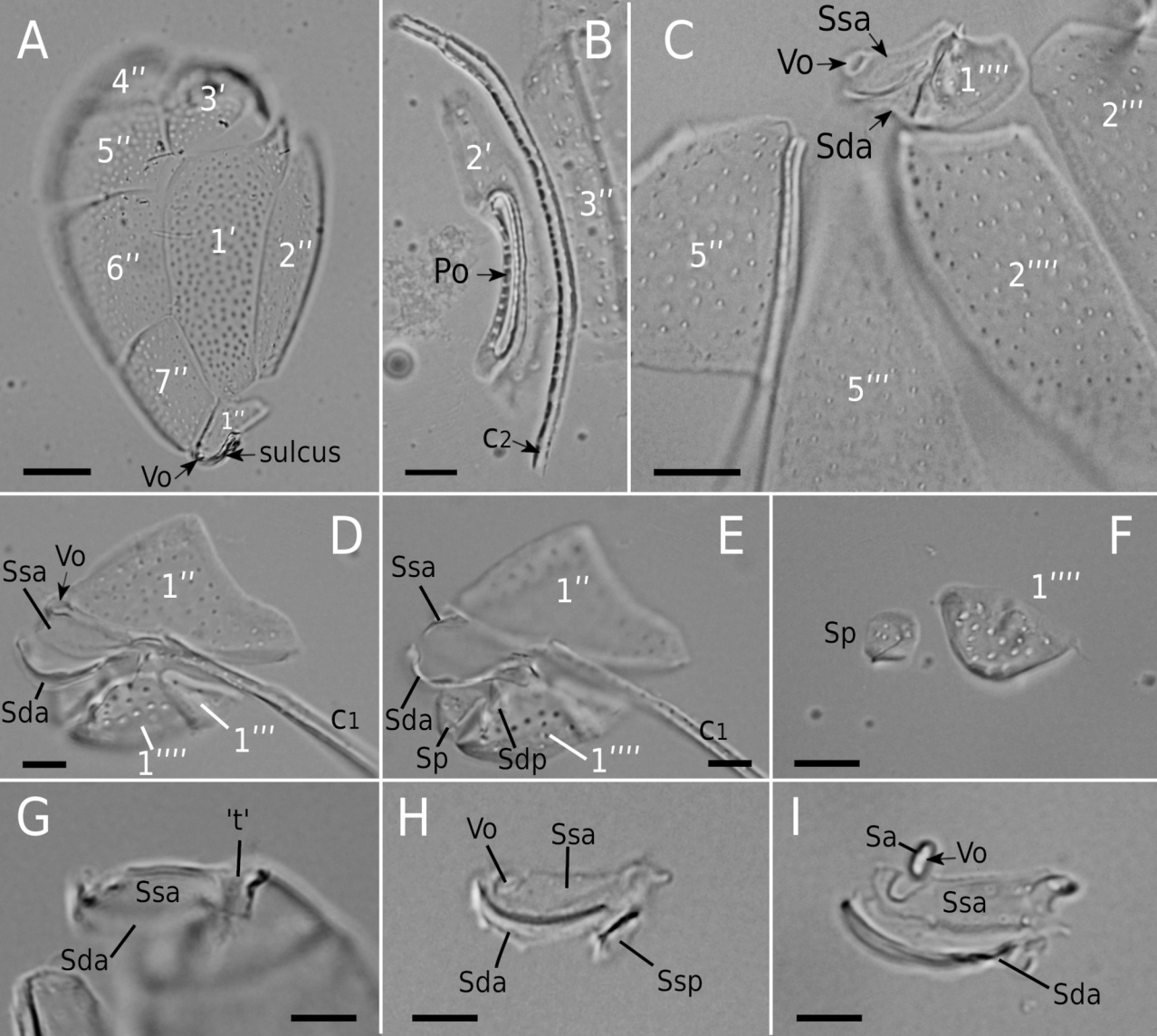
973  
974 **Fig. 10.** Maximum-Likelihood phylogenetic tree based on 49 sequences of small ribosomal SSU  
975 and internal transcribed spacer 1 (2354 aligned characters) of *Amoebophrya* spp. and parasitoid  
976 dinoflagellates (Syndiniales). The clade including the four new sequences found in infected  
977 *Ostreopsis* cells (in bold type) is highlighted with a grey background. Branch robustness was  
978 indicated by bootstrap values (ML) and posterior probabilities (BI). Bootstraps values below 65 and  
979 posterior probabilities below 0.9 are indicated with '-'.

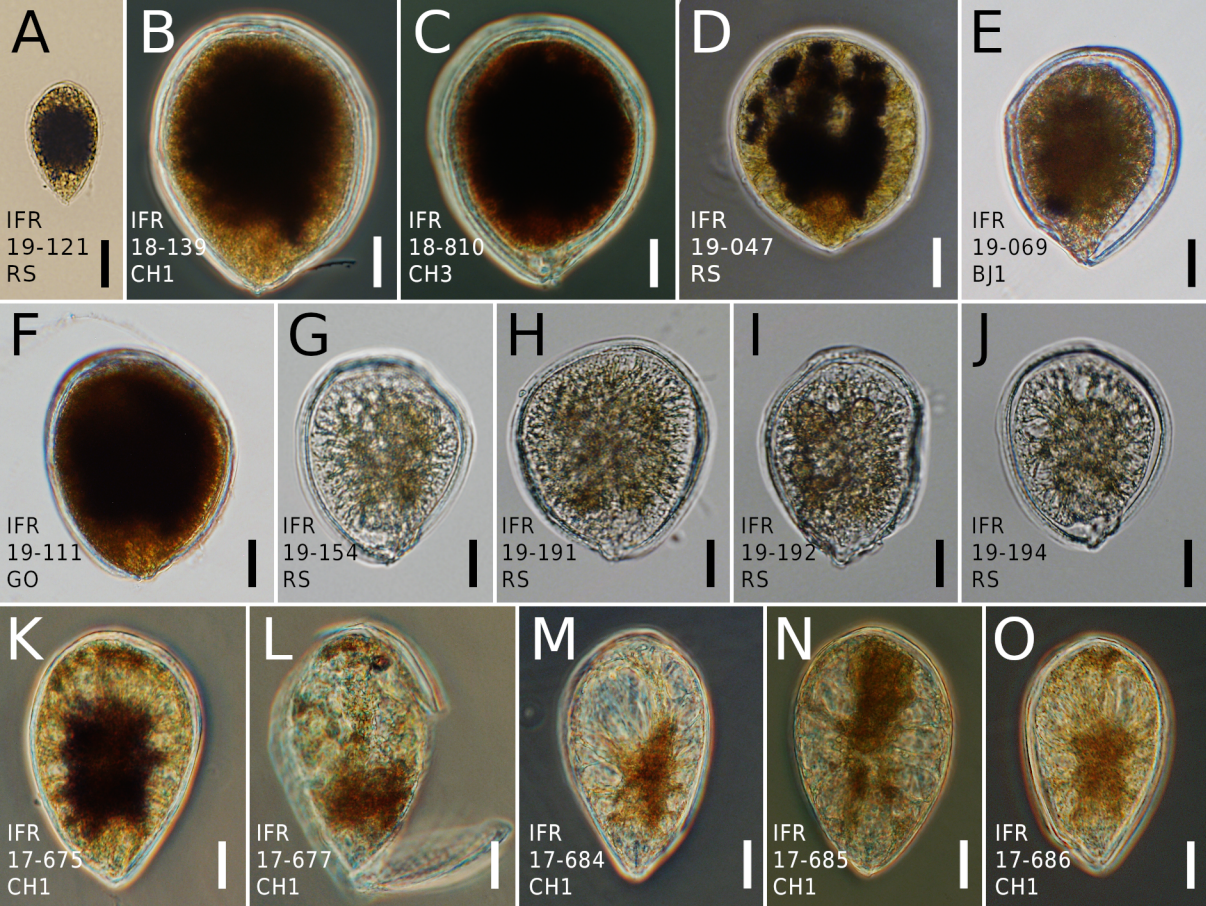






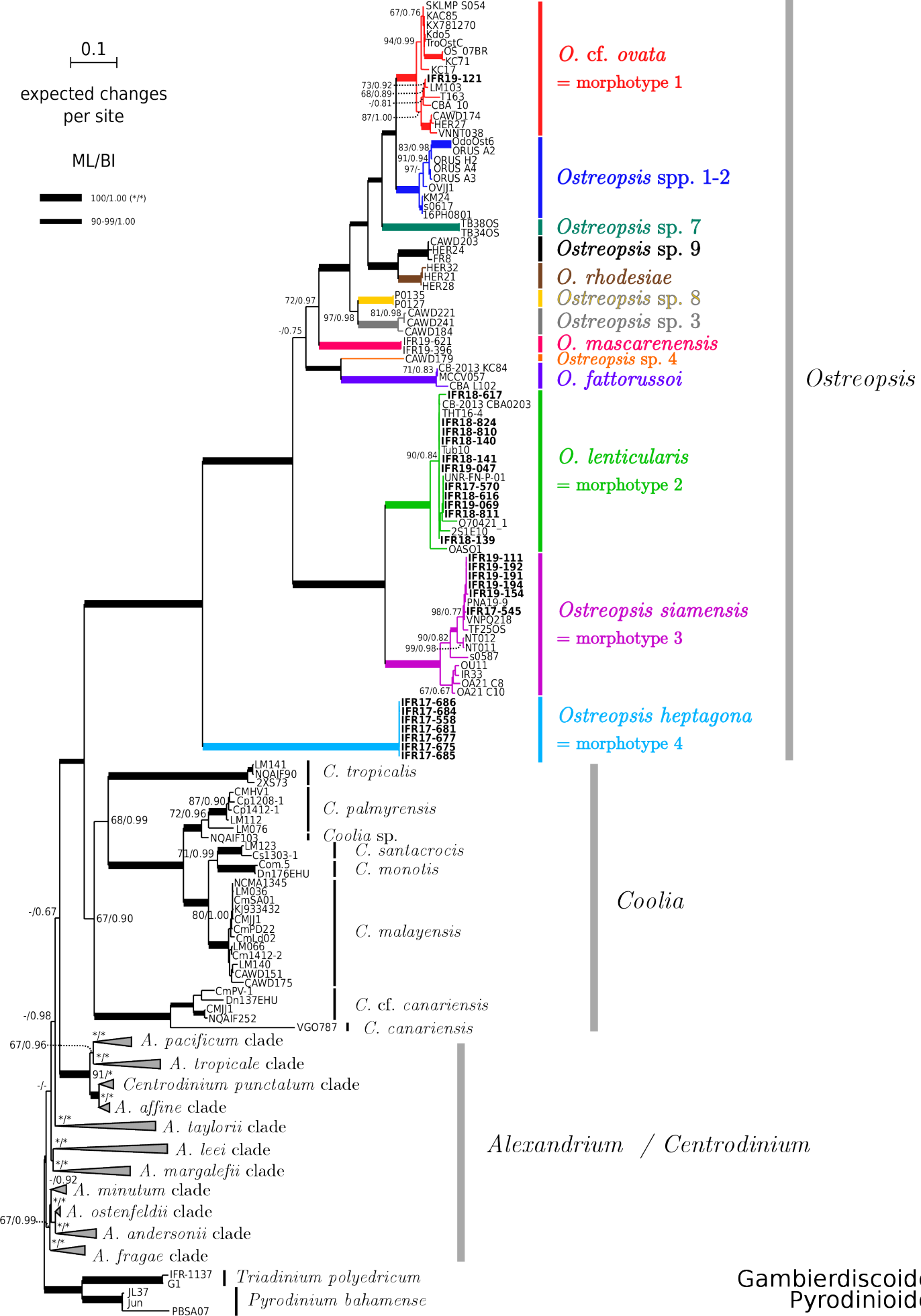






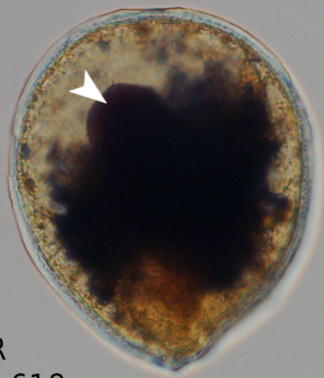
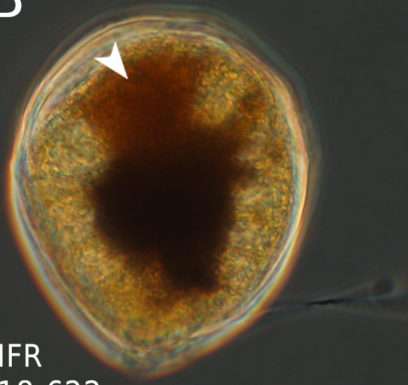
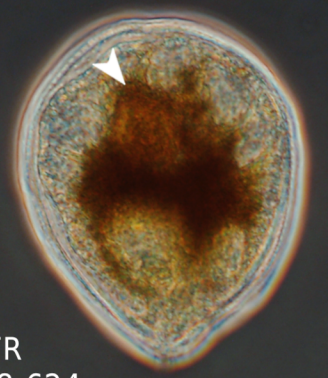
0.1  
expected changes  
per site

ML/BI  
100/1.00 (\*\*)  
90-99/1.00



Ostreopsidoideae

Gambierdiscoideae  
Pyrodinioideae

**A**IFR  
18-618**B**IFR  
18-622**C**IFR  
18-624**D****E****F**